DELFT UNIVERSITY OF TECHNOLOGY

FACULTY OF MECHANICAL, MARITIME, AND MATERIALS ENGINEERING

IMU-BASED ADAPTIVE FILTERING FOR MOVEMENT ARTIFACT REMOVAL FROM ECG RECORDED WITH A SINGLE LEAD WEARABLE DEVICE

BY: CESAR EDUARDO CORNEJO RAMIREZ

STUDENT NUMBER: 5247195

FOR THE DEGREE

MASTER OF SCIENCES IN BIOMEDICAL ENGINEERING

MEDICAL DEVICES TRACK

TU DELFT SUPERVISOR: BORBALA HUNYADI
PRAXA SENSE SUPERVISOR: POURYA OMIDI

DELFT, NETHERLANDS

OCTOBER 07, 2022

Abstract

Background and Objectives: Wearable devices (WDs) capable of recording electrocardiograms (ECGs) for prolonged periods in ambulatory settings offer the possibility of detecting non-predictable events such as epileptic seizures and atrial fibrillation. Nevertheless, these systems suffer from additional noise sources, such as movement artifacts (MA).

Several adaptive (AF) algorithms have been proposed in the literature to suppress movement artifacts from ECG without consistent results. Adaptive algorithms for signal enhancement require a reference signal correlated with the noise and not correlated with the signal of interest. This correlation can change significantly depending on the absolute and relative location of the electrodes and the location of the reference sensor (i.e., accelerometer, gyroscope); objectively measuring the correlation is not a trivial problem.

For this reason, first, we used an algorithm to obtain a rough estimate of the movement artifacts from the recorded ECG to calculate the correlation between them and the available reference signals (three-axis accelerometer and three-axis gyroscope) and selected the one with the highest correlation. Then, we compare three adaptive filter algorithms using the signal-to-noise ratio (SNR) coefficient as the evaluation parameter.

Methods: For testing the implemented adaptive filters, first, we used a simulated signal, then data from an open-online database, and last, a single lead ECG wearable device called AFi® (Praxa Sense™, The Netherlands) with an embedded IMU. To induce the movement artifacts in a controlled setting, participants performed a set of predefined movements within three intensities; high (running, jumping), moderate (torso rotations, pushups), and low (walking). Then we analyzed the recorded data offline as follows:

1. Test the correlation between noise and the IMU components, and select the component with the highest correlation to be used as a reference input for the adaptive filters.
2. Compare three adaptive filters in terms of SNR improvement; the Least means squares (LMS), the Normalized least means squares (NLMS), and the Recursive least squares RLS.
3. Filter the selected reference input with wavelet decomposition, and test if there is a filter performance improvement in SNR.

Results: The implemented adaptive filters performed as expected with the simulated signals, but they showed very poor results once we used them on real data.

The RLS filter showed superior performance than the least mean squares-based filters in terms of convergence speed and the root mean squared error minimization. Nevertheless, it requires a high correlation (ρ) above $\rho>0.8$ between the reference input and the undesired signal or noise to provide a proper signal enhancement and morphology recovery.

The low correlation between the movement artifacts and the components of the IMU used as a reference input for the adaptive filters affected the filter performance heavily. Filtering the reference input with the wavelet decomposition did not improve the correlation or the filter performance.

Conclusions The correlation between ECG motion artifacts and movement recorded with inertial sensors appeared to be low and inconsistent. Given this, adaptive filters using inertial sensors as reference input are unsuitable for removing ECG movement artifacts.

Research Objectives:

- Implement an adaptive filter algorithm to reduce motion artifacts from single-lead ECG recorded with a wearable device, using movement recorded with the integrated IMU.
  - Test the implemented filters with simulated data to evaluate their performance in a controlled setting and under ideal conditions.
  - Develop a methodology to assess the correlation between motion artifacts and movement recorded with the 3-axis from the integrated accelerometer and gyroscope to select the best reference for the adaptive filters.
  - Implement a preprocessing technique to enhance the correlation between movement artifacts and the different axis from the accelerometer and gyroscope.
  - Test and evaluate the algorithm with data gathered with a single lead ECG wearable device and its embedded IMU, and test the same algorithms with data from an open online database.

Index

Abbreviations

- **ACC:** Accelerometer
- **ACCX:** X-axis acceleration
- **ACCY:** Y-axis acceleration
- **ACCZ:** Z-axis acceleration
- **AF:** Adaptive filter
- **AVM:** Acceleration Vector Magnitude
- **ECG:** Electrocardiogram
- **EMG:** Electromyography
- **FIR:** Finite Impulse Response
- **FFT**: Fast Fourier Transform
- **GYR:** Gyroscope
- **GX:** Angular speed around the x-axis
- **GY:** Angular speed around the y-axis
- **GZ:** Angular speed around the z-axis
- **HRV**: Heart Rate Variability
- **IMU:** Inertial Measurement Unit
- **ICA:** Independent Component Analysis
- **LMS:** Least Means Squares
- **MA:** Movement Artifacts
- **MSE:** Mean square error
- **NLMS:** Normalized least means squares
- **RMSE:** Root Mean Squared Error
- **RLS:** Recursive Least Squares
- **SNR:** Signal-to-Noise Ratio
- **UF:** Unfiltered
- **WD:** Wearable Device
- **WSS:** Wide Sense Stationary
- **WSMA:** Weighed Synchronized Moving Average

1. Background

The electrocardiogram (ECG) is the electrical manifestation of the contractile activity of the heart. The ECG combines the action potentials generated by nodal and contractive cells. The electrical currents generated by the heart cells and transmitted through the body can be recorded on the skin surface with electrodes placed at various sites on the body, forming bipolar leads that measure potential differences. A typical ECG has three prominent distinguishable waves or deflections: the P wave, the QRS complex, and the T wave, as shown in Figure 1 [1].

In a healthy heart, the amplitude, duration, and timing of the characteristic deflection and segments tend to be consistent. The ECG is an important diagnostic tool; changes in timing and patterns may evidence problems with the heart's electrical conduction system after a diseased or damaged heart. For example, an elevated or depressed ST segment indicates myocardial ischemia, a prolonged Q-T interval shows a repolarization abnormality that increases the risk of ventricular arrhythmias, and an enlarged R could evidence enlarged ventricles [1], [2].

The heart is situated from an electrical point of view at the center of the electrical field it generates; the intensity of the electric field decreases with the distance from its origin. To provide a comprehensive picture of the heart's electrical activity a 12-lead electrode system is normally used [1], [3].

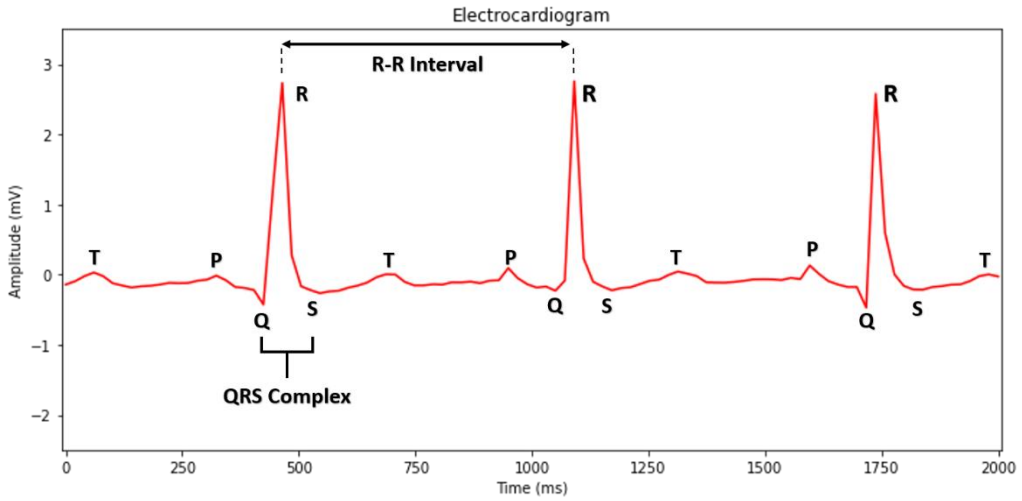

Figure 1. ECG tracing with characteristic deflections, waves, and intervals.

Long-term ECG recordings allow for tracking abnormal cardiac cycles and arrhythmias that occur very sporadically or under particular circumstances, which can detect non-predictable events such as epileptic seizures and atrial fibrillation. The examination lasts 12 hours or more; patients must be connected to stationary monitor stations during this time. Holter monitors, which are portable multiple-lead electrocardiographs, offer patients extra freedom allowing making recordings continuously, even in a home setting [4].

Wearable devices have advantages over Holter monitors for long-term ECG recordings in ambulatory settings. WDs are usually smaller and less obtrusive and have fewer leads, which reduces the preparation time, and in some cases, could be installed without the need for a healthcare professional. For these reasons, WD could make continuous ECG monitoring less cumbersome and expensive [5].

Figure 2. Single-lead ECG Wearable device AFi® with a self-adhesive Ag/Cl electrode.

ECG wearable devices could record cardiac activity while the subject performs routine physical activities in their natural environments and for extended periods. Nevertheless, the extra freedom that WDs provides comes with drawbacks, as the occurrence of noise sources like movement artifacts increases with higher activity levels [6], [7].

1.1 Noise sources in ambulatory electrocardiogram

The electrocardiogram is normally corrupted with artifacts and interference from different sources, which are physiological or external; knowing the origin is the first step to avoiding filtering them properly [3], [8]. This section will briefly describe the main noise sources affecting ECG in ambulatory settings and some mitigation techniques.

Power line interference: Power line interference (Figure 3A) manifests as a 50/60Hz signal (depending on the local power supply) that enters the body through electrical and magnetic fields. Skin abrasion and shielding of the cable leads can reduce the effect; additionally, frequency band-stop filters at the corresponding frequency diminishes the problem [8].

Electromyography (EMG) Noise: Combined action potentials from muscles close to the recording electrodes appear over the desired ECG with high-frequency spikes, as shown in Figure 3B. Normal electrode locations for stationary recordings are useless for ECG testing during exercise (Stress testing). Choosing alternative electrode placements can diminish this effect by avoiding big muscle groups [8].

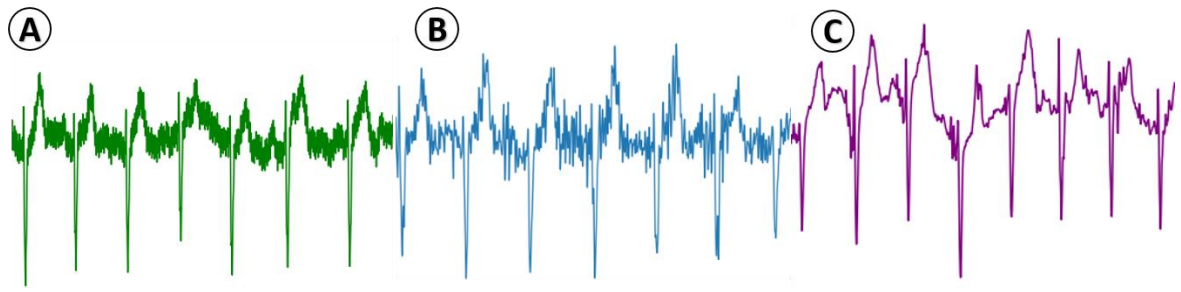

Figure 3. A) ECG corrupted with power line interference, B) ECG corrupted with muscle artifacts, C) ECG corrupted with motion artifacts.

Cable motion: During movement, triboelectric noise is generated by friction and deformation of the insulation of the electrode-leads cables. Low-noise cables with a conductive plastic coating between the conductors and the dielectric minimize the electric noise. Additionally, battery-powered units gain operational amplifiers at each electrode to cancel the effect due to their low impedance [8].

Static electricity: Synthetic clothing during low humidity generates friction-induced discharges. Patient movement generates small currents manifest in the recordings as voltage peaks due to skin impedance under one or more electrodes. Skin abrasion can reduce this problem [8].

Motion artifacts: Motion Artifacts (MA) originate from skin potential changes generated during movement and from the electrode-tissue interface (Figure 3C), a more detailed explanation is provided in the following section [8].

1.2 Movement Artifacts

Movement Artifacts (MA) can reduce ECG signal quality significantly, making ECG interpretation very difficult, and causing diagnostic errors from false detection of arrhythmias and pathological conditions such as atrial fibrillation and flutter [6], [9], [10]. Moreover, MA can bury ECG recordings completely, impeding automatic algorithms from detecting QRS complex properly. As a consequence, features that depend on the correct identification of QRS complex as Heart Rate Variability (HRV) could be incorrectly determined by missing only two heartbeats [3], [11].

Motion-induced artifacts originate from skin-potential variations and changes in the electrode-skin interface during physical activities [8], [9]. When skin stretches, the potential decreases and electrode movements concerning the body produce stochastic skin tension-compression cycles that manifest in random undesired components superimposed on electrocardiogram recordings. Skin abrasion help reduce skin potential changes by scratching the skin barrier layer and short-circuiting the skin potential; nevertheless, it produces irritation and is only a temporary solution as the barrier regrows after about 24 hours [8].

Movement artifacts manifest as spikes and baseline wander shifts that vary depending on the electrode position and physical activity. Figure 4 exemplifies this clearly with three ECG measurements recorded at the same time from different places in the chest; as we can see, the baseline wander and the noise level is different between each lead [12]–[14].

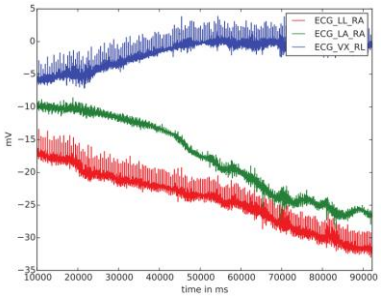

Figure 4. ECG with Baseline-wander recorded from three different locations in the chest. (From [14]**)**

Noise filtering requires different approaches depending on the source. Several noise sources can be effectively suppressed by applying linear digital filters; however, as motion artifacts and ECG frequencies overlap, it is impossible to use frequency-based filters without removing relevant information [9].

Current research in motion artifact removal is divided into three main lines (one hardware-based and two software-based). The first focuses on the electrode skin interface to eliminate motion artifacts from the primary source. The second is based on statistical signal processing methods like Independent Component Analysis (ICA); this method requires multiple channels, which are not always available in wearable settings [7], [15].

The third group joins all adaptive filters, which rely on measuring an auxiliary signal correlated with the motion artifacts but uncorrelated with the heart's electrical activity [16]. This work focuses on the third one, specifically in adaptive filters that use inertial measurement sensors as reference signals.

1.3 Adaptive filtering (AF)

Adaptive filters are non-linear filters whose coefficients are continuously updated using information available in the environment to meet predefined conditions. Adaptive filters are suitable for tracking fast-changing interferences from non-stationary signals as they update continuously, adapting to the characteristics of the signal and the interference [2]. This type of filter has been successfully used in many biomedical applications, for example: canceling the donor ECG in heart-transplant electrocardiography, filtering maternal heartbeat in fetal ECG, suppressing radio frequency interference on ECG due to electrosurgical units, and more [2], [8], [17], [18].

Adaptive filters for signal enhancement use the main input containing the corrupted signal and a reference input correlated in some unknown way with the noise from the main input. The filter modifies the reference signal each iteration and subtracts it from the main input to obtain an estimation of the noiseless main input; as a result, the noise is eliminated or attenuated [17].

Figure 5 illustrates the typical block diagram of an adaptive filter for signal enhancement in the particular case of motion artifact removal. The main input signal $d(k)$ would be the clean ECG $s(k)$ corrupted by motion-related noise $n(k)$, and the input of the adaptive filter a measurable reference from $r(k)$ closely related or correlated with the noise $n(k)$, but uncorrelated with the ECG $s(k)$. In our particular case, we will use a component of the IMU sensor as the reference $r(k)$ as we consider it complies with the two previous requisites.

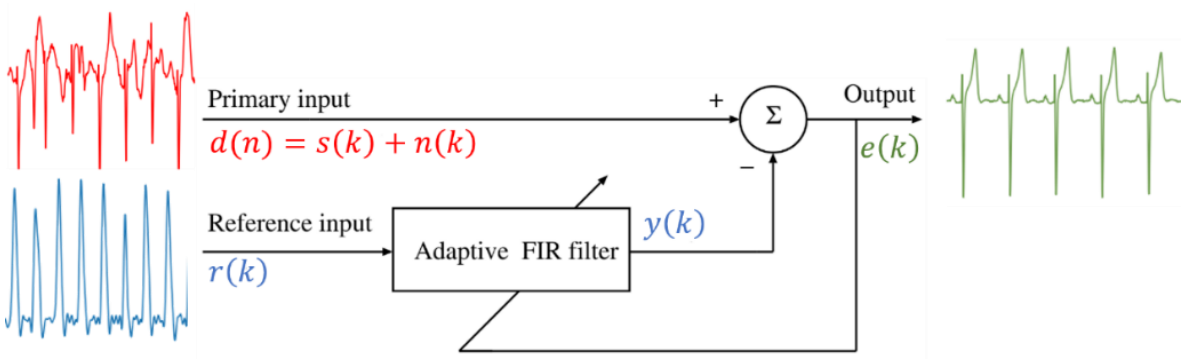

Figure 5. Typical block diagram of adaptive filters for signal enhancement (Adapted from [18]**).**

The error $e(k)$, that in this application is the desired clean signal is given by:

$$e(k) = d(k) - y(k) \tag{1}$$

$$e(k) = s(k) + n(k) - y(k) \tag{2}$$

The adaptive Finite Impulse Response (FIR) filter modifies the reference input $r(k)$ to obtain a signal $y(k)$ as close as possible to the noise $n(k)$. Then $y(k)$ is subtracted from the primary input to estimate the desired signal $\hat{s}(k)$.

$$\hat{s}(k) = e(k) = s(k) + n(k) - y(k) \tag{3}$$

Since $s(k)$ is uncorrelated with n(k) and $r(k)$, the three signals are statically stationary and have zero means. By taking the square of the expectation, the MSE would be then[1]:

$$E[e^2(k)] = E[s^2(k)] + E\{[n(k) - y(k)]^2\} \tag{4}$$

The objective of the filter is to obtain an output $e(k)$ that fits the desired signal $s(k)$ in the least-squares fit sense, the filter feedback the output error to minimize the total system output power[2].

Since minimizing the total output power minimizes the output noise power, minimizing $E[e^2(k)]$ minimizes $E\{[n(k) - y(k)]^2\}$. The output power is minimum when $\xi_{min} = E[e^2(k)] = E[s^2(k)]$, this condition will be met when $E\{[n(k) - y(k)]^2\} = 0$. Since the component $s(k)$ remains unaffected, minimizing the output maximizes the output SNR.

The output of the filter $y(k)$ having an input $r(k)$, can be expressed as:

$$y(k) = \sum_{l=0}^{N-1} \boldsymbol{w}_l \boldsymbol{r}(k-l) \tag{5}$$

Where $k = 0,1,2,\cdots,N-1$ being N the order of the filter, and w_l a tap-weighed vector. From the previous equation (5), we can rewrite the output of the filter at the instant k considering the tap-weighed vectors $\boldsymbol{w}(k) = [w_0(k), w_1(k) \ \cdots \ w_{N-1}(k)]^T$ and the input vector $\boldsymbol{r}(k) = [r(k), r(k-1) \ \cdots \ , r(k-N+1)]^T$ as follows[2]:

[1] By $E[.]$ we refer to the expectation operator.

[2] By $(.)^T$ we refer to the transposed operator, and bold characters **b** represents vectors.

$$y(k) = \boldsymbol{w}^T(k)\boldsymbol{r}(k) \quad (6)$$

Then the estimation error taking the equation (1) will be:

$$e(k) = d(k) - \boldsymbol{w}^T(k)\boldsymbol{r}(k) \quad (7)$$

Several adaptive filter methods are available to optimize the filter and maximize the output SNR, like the Least Means Squares (LMS) and the recursive least squares (RLS), which will be described in the following sections. First, we will describe the Wiener solution, which is the basis of adaptive filters. The Wiener solution provides an optimal filter considering the statistical characteristics of the signal and the noise process, optimizing the filter parameters with an objective function or performance criterion [2].

1.3.1 The Wiener Filter

The Wiener solution minimizes the difference between the input and the estimated reference signal by using the mean-square error (MSE) as an objective function $\xi(k)$ defined as:

$$\xi(k) = E[e^2(k)] \quad (8)$$

Figure 6 shows the schematic representation of an adaptive filter in the direct form of a Finite Impulse Response (FIR) filter structure. Where $y(k)$ is the result after applying the FIR filter to the input signal r(k) and $d(k)$ and e(k) are the desired and error signal respectively [18]. The output signal $y(k)$ is considered an estimate of the desired signal $d(k)$ [2], [18].

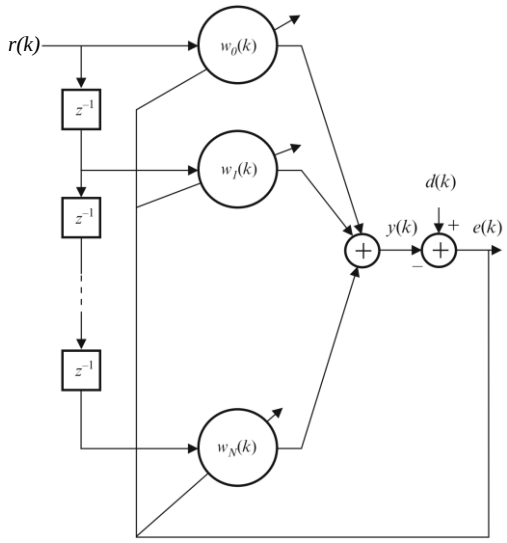

Figure 6 Block diagram of an Adaptive FIR filter (Modified from [18]**)**

If we assume that the desired signal is available, we can calculate an estimation of the error between the output and the desired signal as follows:

$$e(k) = d(k) - y(k) \quad (9)$$

The output of the linear FIR filter can be expressed as the convolution of the input and the tap-weighed vector $\boldsymbol{w}(k)$ as follows:

$$y(k) = \sum_{i=0}^{N} w_i(k) r_i(k) = \boldsymbol{w}^T(k)\boldsymbol{r}(k) \quad (10)$$

Then the estimation error is given by:

$$e(k) = d(k) - \boldsymbol{w}^{\boldsymbol{T}}(k)\boldsymbol{r}(k) \quad (11)$$

Where the input vector $\boldsymbol{r}(k) = [r(k)\, r(k-1)\, \cdots\, r(k-N)]^T$ represents a tap-delay line, and $\boldsymbol{w}(k) = [w_0(k)\, w_1(k)\, \cdots\, w_N(k)]^T$ the tap-weigh vector is also the filter's impulse response [2], [18]. The Wiener filter estimates the tap-weights that minimize the mean square value of the estimated error; then, the output will be the minimum mean squared error estimate of the desired response [2]. The objective function can be rewritten as:

$$\begin{aligned} \xi(k) &= E[e^2(k)] \\ &= E[d^2(k) - 2d(k)\boldsymbol{w}^T(k)\boldsymbol{r}(k) + \boldsymbol{w}^T(k)\boldsymbol{r}(k)\boldsymbol{r}^T(k)\boldsymbol{w}(k)] \\ &= E[d^2(k)] - 2E[d(k)\boldsymbol{w}^T(k)\boldsymbol{r}(k)] + E[\boldsymbol{w}^T(k)\boldsymbol{r}(k)\boldsymbol{r}^T(k)\boldsymbol{w}(k)] \end{aligned} \quad (12)$$

Under the assumption that the input vector $r(k)$ and the desired response $\mathrm{d}(k)$ are jointly Wide-Sense Stationary (WSS)[3], and the tap-coefficient vector $\boldsymbol{w}$ a non-random variable, the MSE can be simplified as follows:

$$\begin{aligned} \xi &= E[d^2(k)] - 2\boldsymbol{w}^T E[d(k)\boldsymbol{r}(k)] + \boldsymbol{w}^T E[\boldsymbol{r}(k)\boldsymbol{r}^T(k)]\boldsymbol{w} \\ \xi &= E[d^2(k)] - 2\boldsymbol{w}^T\boldsymbol{p} + \boldsymbol{w}^T\boldsymbol{R}\boldsymbol{w} \\ Being \quad \boldsymbol{p} &= E[d(k)\boldsymbol{r}(k)] \quad and \quad \boldsymbol{R} = E[\boldsymbol{r}(k)\boldsymbol{r}^T(k)] \end{aligned} \quad (13)$$

Where ξ is a quadratic function of the tap-weighed coefficients, $E[d^2(k)]$ is the variance of $d(k)$,[4] and $\boldsymbol{p}$ is the cross-correlation vector between the desired and the input signal, while $\boldsymbol{R}$ is the input signal autocorrelation matrix. If $\boldsymbol{p}$ and $\boldsymbol{R}$ matrix are known, the solution for $\boldsymbol{w}$ would be minimizing ξ.

$$\begin{aligned} \boldsymbol{g}_{\boldsymbol{w}} = \frac{\partial \xi}{\partial \boldsymbol{w}} &= \left[\frac{\partial \xi}{\partial \boldsymbol{w}_0}\ \frac{\partial \xi}{\partial \boldsymbol{w}_1} \cdots \frac{\partial \xi}{\partial \boldsymbol{w}_N}\right]^T \\ g_w &= -\boldsymbol{2}p + \boldsymbol{2}Rw \end{aligned} \quad (14)$$

By equating the gradient vector of the MSE function $\boldsymbol{g}_{\boldsymbol{w}}$ to zero (with the assumption that the signal $d(k)$ has zero means) the optimal values that minimize the objective function can be evaluated with the so-called Wiener-Hopf solution:

$$w_0 = R^{-1}p \quad (15)$$

The Wiener solution is the theoretical optimal solution; however, in a natural system is not always achievable; nevertheless, some algorithms converge to the Weiner solution, as the LMS introduced in the next section [6], [18].

1.3.2 Least Means Squares (LMS)

[3] Two processes are WSS if any linear combination of them is also WSS, this property implies that both have shift invariant means and their autocorrelation and cross-correlation is shift invariant [18].

[4] The variance of $d(k)$ can be written as σ_d^2

The LMS algorithm is one of the most widely used adaptive filtering algorithms. Its main features are low computational complexity, stable behavior, and converge to the Weiner solution in stationary environments when the input vectors are uncorrelated over time [2], [18].

The LMS updating equation comes from the optimal Wiener solution using a steepest-descent-based algorithm [2], [18]. Adaptive filters aim to minimize the MSE by adjusting a tap-weight vector if we square the error estimation from equation (7).

$$e^2(k) = d^2(k) - 2d(k)\boldsymbol{r}^T(k)\boldsymbol{w}(k) + \boldsymbol{w}^T(k)\boldsymbol{r}(k)\boldsymbol{r}^T(k)\boldsymbol{w}(k) \quad \textbf{(16)}$$

The squared error is a second-order function, and its geometrical interpretation is a concave paraboloid surface (Figure 7). The objective of the optimization procedure would be to reach the minimum of the function with the steepest-descent-based method [2].

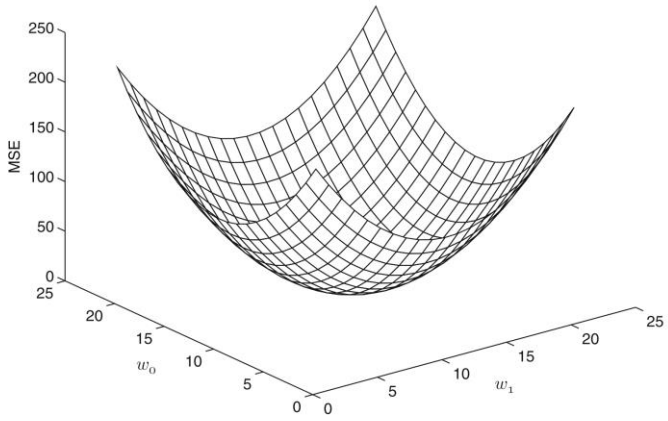

Figure 7. Mean square error surface (from [18]**).**

In the steepest-descent method, the new vector $\mathbf{w}(k+1)$ is obtained with the previous vector $\boldsymbol{w}(k)$ and a correction factor proportional to the negative of the gradient of the squared error $\nabla e^2(k)$:

$$\mathbf{w}(k+1) = \boldsymbol{w}(k) - \mu\nabla e^2(k) \quad \textbf{(17)}$$

The constant μ is the convergence factor and controls the stability and rate of convergence of the filter. The estimate of the gradient can be obtained by the derivate of the gradient of the squared error with respect to the weight vector from equation (17) as:

$$\widetilde{\nabla e^2}(k) = -2d(k)\boldsymbol{r}(k) + 2\{\boldsymbol{w}^T(k)\boldsymbol{r}(k)\}\boldsymbol{r}(k) = -2e(k)\boldsymbol{r}(k) \quad \textbf{(18)}$$

Replacing the estimate of the gradient in equation (17).

$$\boldsymbol{w}(k+1) = \boldsymbol{w}(k) - 2\mu e(k)\boldsymbol{r}(k) \quad \textbf{(19)}$$

Equation (19) is the updating equation of the Widrow-Hoff LMS algorithm.

The convergence speed of the LMS depends on the eigenvalue spread of the input-signal autocorrelation matrix R. The filter converges to the Wiener solution if a convergence factor μ is chosen according to the following inequality.

$$0 < \mu < \frac{2}{\lambda_{max}} \quad \textbf{(20)}$$

Where λ_{max} corresponds to the maximum eigenvalue of the autocorrelation matrix R.

The convergence factor μ influences the filter performance significantly; a large convergence factor increases convergence speed but turns the filter response more sensible, even to marginal variations of the reference signal. Conversely, a small convergence factor could fail to track fast-changing motion artifacts or make the filter not affect the original signal [19]. In summary, the convergence factor has to be chosen carefully to balance stability and speed [12], [13].

Several algorithms originate from the conventional LMS; their objective is either to reduce computational complexity or convergence time [18]. One of those is the Normalized Least Means Squares (NLMS); in this algorithm, the convergence factor varies with time, providing better stability and faster convergence [18].

1.3.3 Normalized Least Means Squares (NLMS)

To increase the convergence speed of the LMS, the NLMS uses a variable convergence factor μ_k that aims the minimization of the instantaneous input error. Then updating the formula of the LMS could be expressed as:

$$\boldsymbol{w}(k+1) = \boldsymbol{w}(k) - 2\mu_k e(k)\boldsymbol{r}(k) \tag{21}$$

The value μ_k has the objective of reaching a faster convergence. A solution would be reducing the instantaneous squared $e^2(k)$ error as much as possible, and it is a simple estimate of the MSE [18]. Then the value of μ_k that makes $\frac{\partial \Delta e^2(k)}{\partial \mu_k} = 0$ is given by:

$$\mu_k = \frac{1}{2\boldsymbol{r}^T(k)\boldsymbol{r}(k)} \tag{22}$$

To control misadjustments, since the derivations are based on instantaneous values of the squared error instead of the MSE, a fixed convergence factor μ_n is included. Additionally, a constant γ to avoid large step sizes if the denominator becomes too small. Introducing the constants and the variable convergence factor μ_k In (21), the updating equation of the filter will be:

$$\boldsymbol{w}(k+1) = \boldsymbol{w}(k) + \frac{\mu_n}{\gamma + \boldsymbol{r}^T(k)\boldsymbol{r}(k)} e(k)\boldsymbol{r}(k) \tag{23}$$

Equation (23) is the updating equation of the Normalized Least means Squares (NLMS) algorithm.

To guarantee stability, the range of values of μ_n has to be chosen between:

$$0 < \mu = \frac{\mu_n}{2tr[\boldsymbol{R}]} < \frac{1}{tr[\boldsymbol{R}]} \tag{24}$$

Where $tr[\boldsymbol{R}]$ is the trace of the input autocorrelation matrix. In practice, the value μ_n can be chosen between $0 < \mu_n \leq 1$ and γ should be a small constant $\gamma"\mu_n$ [18].

The LMS and NLMS are both simple and efficient approaches for quasistationary systems, with good steady-state performances. However, with fast varying signals, a fast adaptation is needed for tracking variations in the

input process efficiently. The Recursive Least Squares method offers an alternative with an exact minimization of the least squares estimate [2], [18].

1.3.4 Recursive Least Squares (RLS)

RLS algorithms could achieve fast convergence even with a large eigenvalue spread of the input signal correlation matrix, which makes them ideal for time-varying environments. Additionally, the rate of convergence of RLS filters is one order of magnitude higher than LMS-based algorithms at the expense of computational complexity and some stability problems [2], [9], [17], [18].

The objective function is given by:

$$\xi^d(k) = \sum_{i=0}^{k} \lambda^{k-i} \varepsilon^2(i) \tag{25}$$

$$= \sum_{i=0}^{k} \lambda^{k-i} \left[d(i) - \boldsymbol{r}^T(i)\boldsymbol{w}(k)\right]^2 \tag{26}$$

The RLS algorithm uses the posteriori error $\varepsilon(k)$ instead of the prior error $e(k)$ and a constant λ that is an exponential weight forgetting factor that makes the information from the past have a decreasing effect in the coefficient update; this value should be selected between $0 < \lambda \leq 1$. The error in equation (26) is the difference between the desired signal and the filter output.

If we differentiate the deterministic, objective function $\xi^d(k)$ with respect to $\boldsymbol{w}(k)$ and equating the result to zero, we can find the optimal vector $\boldsymbol{w}(k)$ that minimizes the least-squares error:

$$\frac{\partial \xi^d(k)}{\partial \boldsymbol{w}(k)} = -2\sum_{i=0}^{k} \lambda^{k-i}\, \boldsymbol{r}(i)\left[\left[d(i) - \boldsymbol{r}^T(i)\boldsymbol{w}(k)\right]\right]$$

$$-\sum_{i=0}^{k} \lambda^{k-i}\, \boldsymbol{r}(i)\boldsymbol{r}^T(i)\boldsymbol{w}(k) + \sum_{i=0}^{k} \lambda^{k-i}\, \boldsymbol{r}(i)\boldsymbol{d}(k) = \begin{bmatrix} 0 \\ \vdots \\ 0 \end{bmatrix}$$

$$\boldsymbol{w}(k) = \left[\sum_{i=0}^{k} \lambda^{k-i}\, \boldsymbol{r}(i)\boldsymbol{r}^T(i)\right]^{-1} \sum_{i=0}^{k} \lambda^{k-i}\, \boldsymbol{x}(i)\boldsymbol{d}(k)$$

$$\boldsymbol{w}(k) = \boldsymbol{R}_D^{-1}(k)\boldsymbol{p}_D(k) \tag{27}$$

From the previous equation $\boldsymbol{R}_D(k)$ is the deterministic correlation matrix and $\boldsymbol{p}_D(k)$ the deterministic cross-correlation vector of the input signal and the desired signal. The inverse of $\boldsymbol{R}_D(k)$ can be simplified by the inversion lemma in the following form [2], [18].

$$\boldsymbol{S}_D(k) = \boldsymbol{R}_D^{-1}(k) = \frac{1}{\lambda}\left[\boldsymbol{S}_D(k-1) - \frac{\boldsymbol{S}_D(k-1)\boldsymbol{r}(k)\boldsymbol{r}^T(k)\boldsymbol{S}_D(k-1)}{\lambda + \boldsymbol{r}^T(k)\boldsymbol{S}_D(k-1)\boldsymbol{r}(k)}\right] \tag{28}$$

The prior error can be defined as:

$$e(k) = d(k) - \boldsymbol{r}^T(k)\,\boldsymbol{w}(k-1) \tag{29}$$

The weight coefficient equation can be expressed as:

$$\boldsymbol{w}(k) = \boldsymbol{w}(k-1) + e(k)\boldsymbol{S}_D(k)\boldsymbol{r}(k) \tag{30}$$

Equation (30) is the updating equation for the weight coefficients for the RLS filter.

1.4 Reference Signals

As we have seen in the previous sections, adaptive filters estimate the noise superimposed to the signal of interest, using a different reference input highly correlated with noise. In statistics, correlation indicates the extent to which two variables fluctuate in relation to each other. In two correlated variables, the magnitude increase or decrease of one variable is associated with a change in the magnitude of another variable, either in the same (positive correlation) or in the opposite direction (negative correlation) [20]. Therefore, for using adaptive filters to remove motion artifacts from ECG, we need a measurable external signal with a strong and consistent correlation with motion artifacts.

Motion artifacts originate from undesired potential changes in the skin generated by stretching during physical activity [8]. We could assume that quantifying skin stretching or the movements that generate tension and compression cycles would provide information about how MA would affect the electrocardiogram. However, the underlying information is not directly available.

There are mainly two approaches to obtaining an adequate reference signal for adaptive filters in the literature. The first is based on measuring body movements with dedicated sensors like Inertial Measurement Units (IMUs) containing accelerometers, gyroscopes, and magnetometers [9]. Several studies have explored this method [4]–[7], [9], [11]–[16], [19], [21]–[36], as IMUs offer several advantages, like low power consumption, small size, and weight and the possibility to integrate them in electronic circuit boards.

The second group focuses on skin-electrode impedance changes, measured directly by introducing a low alternate current with the recording electrodes or indirectly with optical sensors that record skin stretching [6], [19], [37].

As stated in the research objectives, in this report, we will focus on inertial reference signals, as these are the sensors available in the wearable device. In the literature, the most used inertial sensors were accelerometers, followed by gyroscopes; nevertheless, there is no consensus on which axis to use as a reference signal for adaptive filters [4]–[7], [9], [11]–[16], [19], [21]–[36].

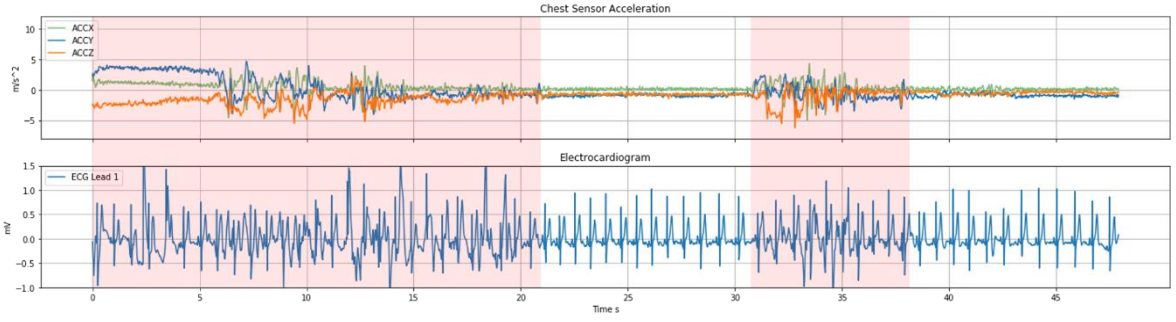

Figure 8. ECG and 3-axis acceleration recorded simultaneously; the red zones enclose the zones with movement.

Raya (2002), Milanesi (2006), Gautam (2008), Yang (2008), Dargie (2016), and Huang (2019) suggested using the y-axis, arguing it contains the highest components of most human movements, as it coincides with the gravity acceleration [12], [14], [15], [28], [30], [33]. Yoon (2008) and Martini (2010) disagreed, stating that the z-axis was a better reference as it represents the normal component of the electrode contact area with the skin, showing disconnections of the electrode from the subject skin [9], [36].

Xiong (2020), Beach (2021), and Lilienthal (2021), instead of choosing a predefined axis, measured the correlation on all components and selected the one with the highest value depending on the particular scenario [16], [19], [21].

If we record acceleration at the same time as ECG during intense movement and plot the signals, we can empirically tell that both have some level of mutual relation, as shown in Figure 8. However, objectively measuring the correlation is not a straightforward problem, as we need the isolated motion artifacts and the reference.

1.5 Correlation

Measuring correlation could be done using MA isolated from ECG, but this is only possible in controlled environments. The results could differ from a real scenario depending on the underlined assumptions. Martini et al. (2010) induced artifacts manually by moving the electrodes, cables, or the skin around one of the electrodes in two lead-ECG recorded at rest while keeping the other lead unaltered, then they subtracted the signal without moving artifacts from the other to obtain an estimation of the motion artifacts [9], [34]. Romero (2012), Lilienthal (2021), and Buxi (2012) recorded isolated movement artifacts from the back of their subjects at the height of the lumbar curve, where they considered the electrical activity of the heart was negligible [6], [19], [32], [37]. The clean ECGs were recorded at rest in these two previous approaches omitting variable heart rate and ECG morphology changes during exercise [38].

An alternative could be calculating the correlation between the reference sensor and noisy ECG [7], [16], [21]. Still, we must remember it would not be comparable with the correlation calculated with isolated MA.

Several aspects like the electrode-skin interface (Ag-AgCl electrodes, dry electrodes, electro-conductive fabric electrodes), skin preparation, and the presence of sweat influence the appearance of movement artifacts and, consequently, modifies the correlation between them and the reference signal [8]. Moreover, as noted by Lilienthal et al., correlation changes depending on the location of the sensor and the physical activity (Figure 9). They found that attaching sensors over or near the location of the ECG electrodes could generate additional disturbances due to the extra weight introduced, modifying the inertial characteristics of the system [14], [19].

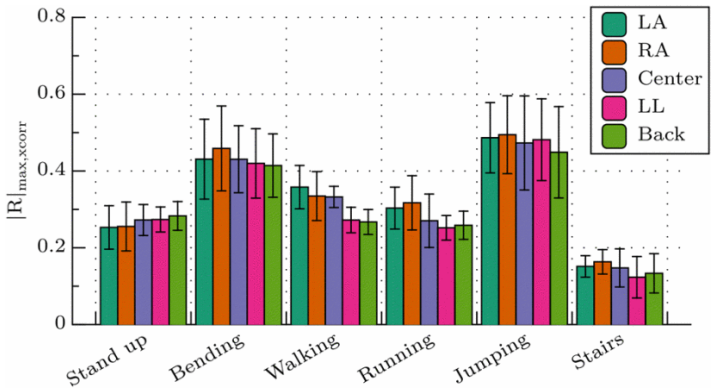

Figure 9. The median maximum cross-correlation coefficient between ECG with movement artifacts and accelerometers located in different body parts (from [19]**).**

A correlation coefficient is a dimensionless quantity between -1 and +1 that indicates the strength of the linear association (Pearson correlation) between two variables. The stronger the correlation, the closer the coefficient comes to ±1 [39]. Adaptive filters rely on the correlation between the reference signal and noise; the higher the correlation, the better estimate of the error signal. Using an uncorrelated reference signal may lead to contaminating the ECG with additional noise [2], [4], [7], [15].

Marini et al. (2010) compared the SNR improvement of LMS and RLS filters depending on the correlation between movement artifacts and the z-axis (perpendicular to the chest) in three-second windows. As we can see in Figure 10, the SNR improvement increased with higher levels of correlation for both RLS and LMS filters [9].

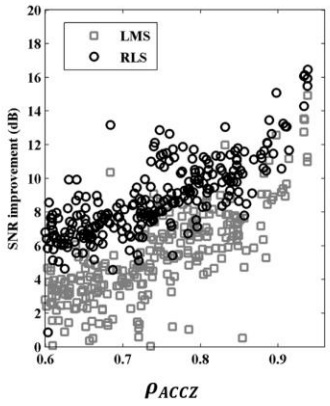

Figure 10. Signal-to-noise ratio improvement of LMS and RLS adaptive filters as a function of the correlation between motion artifacts and the accelerometer z-axis, only correlation values above 0.6 are shown (modified from [9]**).**

1.6 Preprocessing

The raw reference signal can be preprocessed with different methods to enhance the unknown mutual relation between noise and the reference signal and reduce the adverse effects of low correlation. One of the most used methods was processing the reference with a band pass filter coincident with the ECG frequency spectrum,

assuming that the power of the signal outside this frequency range won't relate to the movement artifacts [5], [9], [19], [21], [32], [35], [40].

Another approach was to combine the different components of the IMU in a single reference; in the case of the accelerometer, this can be done by calculating the Acceleration Vector Magnitude (AVM) [7], [22], [27], [29].

$$\mathrm{AVM} = \sqrt{\mathrm{ACCX}^2 + \mathrm{ACCY}^2 + \mathrm{ACCZ}^2} \quad (31)$$

Pandey et al. (2010) [24] combined the 3-axis of an accelerometer applying the fast Fourier transform to each component and then added them with the inverse Fourier transform. He hypothesized that ECG baseline drifts due to motion artifacts proceeding from complex body motions that would be only captured with a multi-axial reference.

Ghaleb et al. (2018) [7] claimed that macroscopic body movements recorded with IMUs do not necessarily have a high correlation with electrode movements in all cases. To tackle this, they proposed a weighted adaptive noise-canceling filter that uses the cross-correlation between the AVM derivative and ECG with MA as updating weight factor. In this way, the impact of the adaptive filter decreases during low correlation conditions.

Instead of using the raw information from IMUs as reference signals, Hostettler et al. (2018) [4] estimated the full 3D short-term electrode motion relative to its stationary position in a common global coordinate system for having a reference invariant to the sensor orientation. Yoon et al. (2008) [36] transformed the acceleration recorded to global coordinates using rotation matrixes before using the signals as a reference for an NLMS filter.

In most cases, the impact of the preprocessing step was not evident, or there was no comparison of the correlation difference with and without the preprocessing. Xiong et al. (2020) were one of the exceptions; first, they compared the correlation between the components of three IMUs located in different parts of the body and the raw ECG and chose the one with the highest correlation. Then they decomposed the selected IMU component with a multiscale wavelet and omitted the wavelet coefficients with the lowest correlation. Lastly, they reconstructed the reference signal with the selected wavelet coefficients; this method improved the correlation and the SNR after using LMS and NLMS adaptive filters (Figure 11) [16].

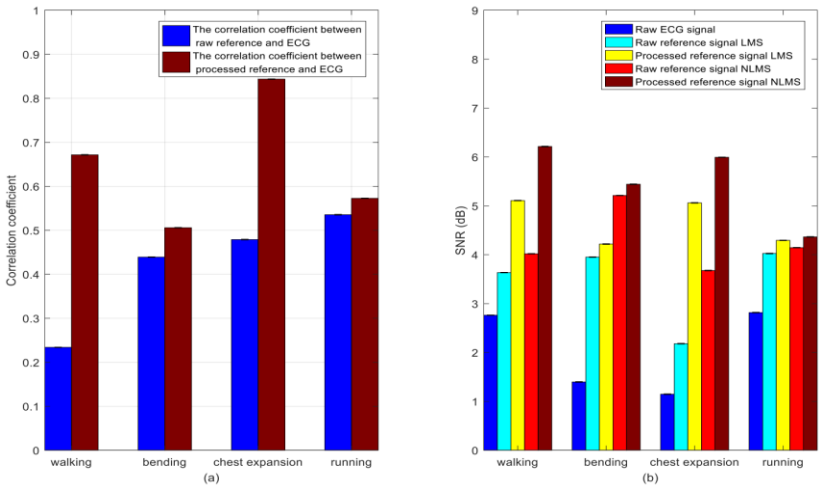

Figure 11. a) Correlation coefficients between raw ECG and the selected reference signal before and after processing with wavelet transform b) SNR before and after filtering with and without processed reference (form [16]**).**

2. Methodology

In this work, we implemented three adaptive filters to compare their performance in removing movement artifacts. First, an LMS filter because it is the most used one in the literature, then an NLMS, an improved version of the first one, and last, an RLS filter. The RLS has better performance for dynamic systems and faster convergence speed than the LMS-based filters at the cost of higher computational load. The mathematical background of the three adaptive filters was developed in the introduction, and the Python-implemented algorithms are in the appendixes. To evaluate the level of improvement after applying the filters, we calculated the Signal-to-Noise Ratio (SNR) as follows:

$$SNR(dB) = 10 \cdot \log_{10}\left(\frac{\sum_{n=1}^{N}[x(n) - \bar{x}]^2}{\sum_{n=1}^{N}[x(n) - \tilde{x}(n)]^2}\right) \quad (32)$$

Where $x(n)$ is the clean ECG signal with a mean value $\bar{x}$, and $\tilde{x}(n)$ the noisy ECG [41].

We tested the AFs in three different setups, starting with simulated signals, then with an open online database, and last on data recorded with the wearable device AFi.

The experiments with the simulated signal offered the possibility to change the correlation values between the noise and the reference input; this is not possible with the recorded data from the database and the wearable device. For this reason, we proposed a method to estimate the correlation with the available data, explained in chapter 2.4.1.

As we have stated multiple times, adaptive filters rely on high correlation values between the reference input and noise; for this reason, we implemented and tested a methodology proposed by Xiong et al. (2020) [16] to enhance the correlation by manipulating the reference signal, explained in chapter 2.4.2.

2.1 Simulated Signal

As a first step, we performed a simulation study to investigate the performance of the three filters under different correlation levels between noise and reference input. The simulated signals were generated with NeuroKit2[5], an open-source Python toolbox for physiological signal processing [42]. First, we created a clean ECG with an average heart rate of 70 beats per minute and a respiratory signal[6] with random noise, both signals with a sampling frequency of 512Hz and 50 seconds in length; then, we added the respiratory signal to the ECG. Figure 12 shows an example where the noise buries the ECG completely with a $SNR = -8.73dB$.

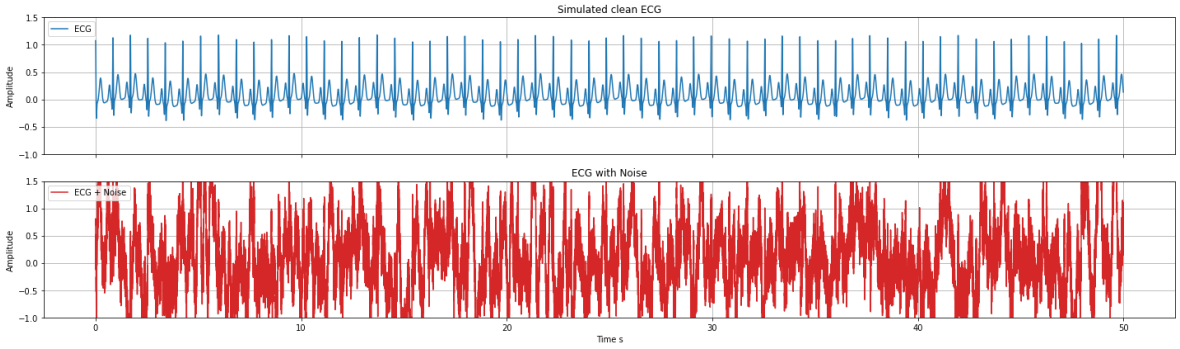

Figure 12. (Top) Simulated clean ECG signal. (Bottom) ECG with respiratory and random noise with an SNR of -8.73dB.

To test the filter's performance under ideal conditions, we used the same signal as noise and as reference input for the adaptive filters (Figure 13); by doing this, the Pearson correlation has the maximum possible value $\rho_{Max} = 1$. Then we decreased the correlation from ρ=1 to ρ=0.8, ρ=0.4, ρ=0.2, and ρ=0.1 by adding every time more random noise to the reference.

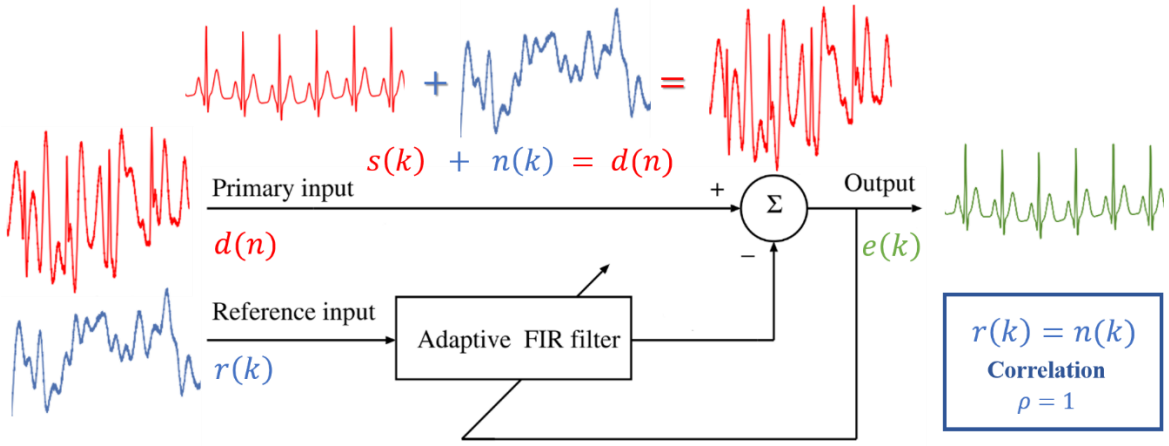

Figure 13. Block diagram of the adaptive filters tested under ideal conditions using the added noise $n(k)$ as reference input $r(k)$, in this way the correlation has the maximum correlation $\rho_{Max} = 1$.

[5] Available at https://neuropsychology.github.io/NeuroKit/ (Las access September 2022)

[6] From the biosignlas available in the toolbox, we selected the respiratory signal as noise source, because was easily customizable (noise level, amplitude, and beats per minute).

2.2 Online Database

We first used an open online database to test the filters on real ECG data. The "MHEALTH dataset"[7] contains recordings between 40 to 60 minutes long from 10 healthy subjects performing twelve different physical activities. The subjects had three inertial sensors, one placed on the right wrist, one around the left ankle, and one over the chest. For our purposes, we only used the sensor over the chest (Figure 14) because it includes a 2-lead ECG and a 3-axis accelerometer recorded simultaneously at a frequency of 50Hz [42], [43].

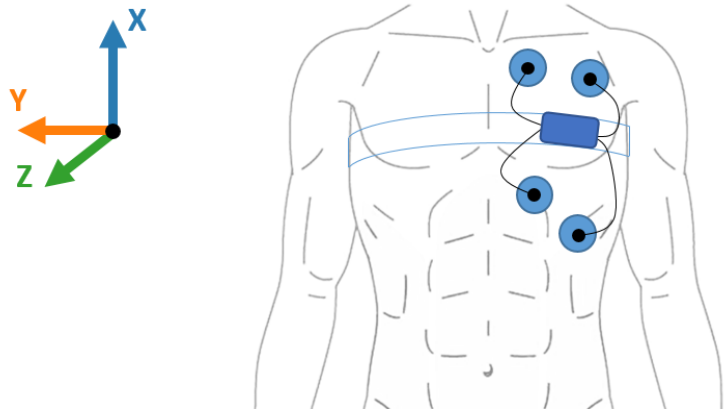

Figure 14. Two-lead ECG and accelerometer are attached to the chest with an elastic band.

For consistency with the experimental setup explained in the following section, from the twelve different activities, we choose two with a high-intensity level (running and jumping), one with a lower level (walking), and one with no displacement (crouching), the activities were either one minute or 20 repetitions. From the two ECG leads, we only used one.

- High Intensity:
  - Jumping 20 times in the same spot.
  - Running without a restricted direction for 60 seconds.
- Low intensity:
  - Walk without a restricted direction for 60 seconds.
- Static position activities:
  - Standing and crouching 20 times in the same spot (squats).

2.3 ECG recorded with a WD

To answer some of the research questions and test the performance of the adaptive filters, we designed an experimental setup using a wearable device developed by PraxaSense® called Afi. The WD contains several sensors, including a single lead electrocardiogram, a temperature sensor, a photoplethysmograph (PPG), and an Inertial Measurement Unit (IMU). The IMU includes a 3-axis accelerometer and a 3-axis gyroscope (Figure

7 Available at: http://archive.ics.uci.edu/ml/datasets/mhealth+dataset (Last access September 2022)

15). The device can record continuously for extended periods with its embedded rechargeable battery, and its small size and weight allow for gathering data unobtrusively in ambulatory settings.

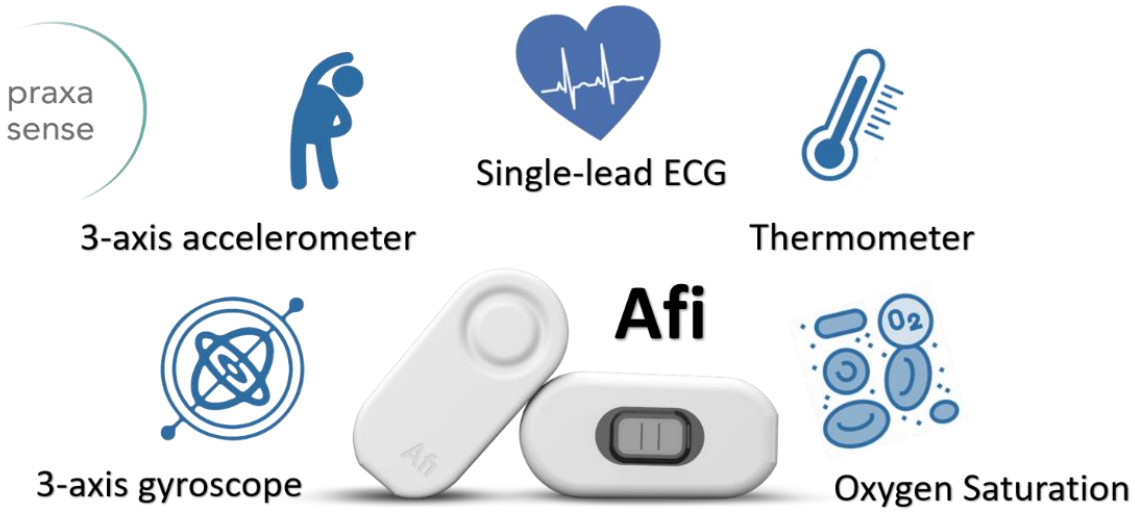

Figure 15. Render of the Single-lead ECG wearable device AFI with the embedded sensors it includes (Modified from [44]**).**

The experiment involved recording the ECG from one volunteer using a wearable device. The participant performed five physical activities for 15 seconds, each with one-minute rest between the activities; two high intensity (jump, run), one with low intensity (walk), and two without displacement, but that would generate skin stretching (torso rotations, pushups).

- High Intensity:
  - Jumping several times in the same spot for 15 seconds.
  - Run in a straight line for 15 seconds.
- Low intensity:
  - Walk without a restricted direction for 15 seconds.
- Static position activities:
  - Torso rotations from left to right, standing straight several times for 15 seconds.
  - Pushups for 15 seconds.

To avoid preventable movement artifacts, the skin was prepared by scratching it with sandpaper (3M Red Dot™ Trace Prep) before sticking the electrodes. To coordinate the starting time of the recordings, a single jump was used as a clapperboard. The device was placed according to the intended use in the middle of the chest at the sternum height (FIGURE 16), and it was attached to the skin with a self-adhesive disposable Ag/AgCl electrode.

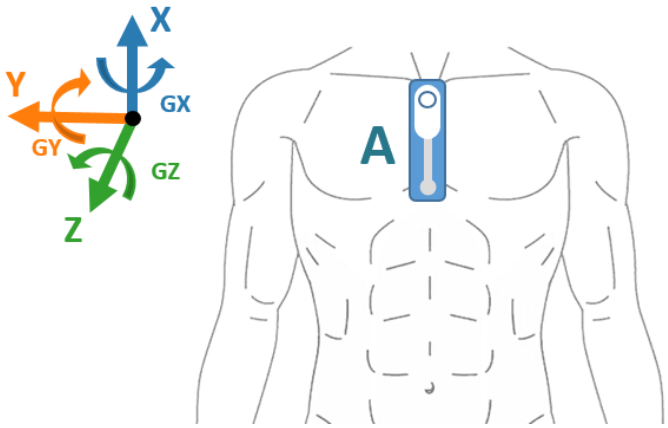

Figure 16. Location of the wearable device over the chest at the sternum height.

2.4 Reference and Correlation

Adaptive filter performance depends on correctly selecting a reference signal correlated with noise. In the literature, accelerometers and gyroscopes have been used by several studies [4]–[7], [9], [11]–[16], [19], [21]–[36]. Nevertheless, there is no consensus on which inertial sensor or component is the best reference for adaptive filters. For this reason, we calculated the correlation between the movement artifacts and the different axis of the accelerometer and the gyroscope to select the one with the highest correlation per activity. However, as the movement artifacts are combined with the ECG, this is not possible directly. Therefore, we proposed a new method using the available data explained in the first part of this chapter (section 2.4.1).

Besides selecting an adequate reference input, the higher the correlation, the better the filter performance. Consequently, to enhance the correlation between movement artifacts and the available reference signal, we decided to test the pre-filter method proposed by Xiong et al. (2020) based on a wavelet transform; described in the second part of this chapter (section 2.4.2) [16].

2.4.1 Weighed Synchronized Moving Average (WSMA) for Noise Extraction

According to our main research objective, we wanted to develop an adaptive filter for a single-lead ECG wearable device. In a real scenario, we will not have access to a clean ECG or isolated movement artifacts. Therefore, we implemented a method with the available information to choose the reference with the highest correlation with the movement artifacts. For that reason, we used a weighted synchronized moving average and an RLS filter to obtain a rough estimation of the movement artifacts. The complete procedure will be described in this section.

Synchronized averaging is a technique used to remove random noise in periodic signals [2], [45]. In a strict sense, the electrocardiogram is not a periodic signal as there are natural variations between each QRS complex, some with clinical relevance; moreover, its morphology and frequency change when performing physical activities [38]. Nevertheless, for our purpose, we can consider it periodic; for this, we have to align consecutive QRS complexes using the R-peaks as the starting point.

One of the restrictions of this method is that each repetition of the periodic signal should have the same length; for this, we calculated the number of samples between R-R intervals and resampled all R-R complexes to the mean R-R length.

Let's consider that $y_k(n)$ represents a complete R-R complex or one realization of the periodic signal with $k = (1,2,3,\cdots,M)$ being M the number of repetitions, the individual samples $n = (0,1,2,3,\cdots,N-1)$ and M the number of samples on each recording. Then the signal of interest $x_k(n)$ with the random noise $\eta_k(n)$ would be:

$$\boldsymbol{y}_k(n) = \boldsymbol{x}_k(n) + \boldsymbol{\eta}_k(n) \tag{33}$$

For each instant, n we add the M copies of the signal:

$$\sum_{k=1}^{M} \boldsymbol{y}_k(n) = \sum_{k=1}^{M} \boldsymbol{x}_k(n) + \sum_{k=1}^{M} \boldsymbol{\eta}_k(n) \tag{34}$$

If all the QRS complexes are identical and aligned $\sum_{k=1}^{M} \boldsymbol{x}_k(n) = M\boldsymbol{x}(n)$, and if the noise is uncorrelated with the signal, with zero mean and variance σ_η^2, the sum of the errors $\sum_{k=1}^{M} \boldsymbol{\eta}_k(n)$ will tend to zero as M increases; the larger the number of averaged cycles, the higher the SNR. After this, we can get a clean average R-R complex $\overline{\boldsymbol{y}_k}$ as follows[2]:

$$\overline{\boldsymbol{y}_k} = \frac{1}{M} \sum_{k=0}^{M-1} \boldsymbol{y}_k(n) \tag{35}$$

Figure 17 shows the electrocardiogram in the recovery state after exercise. As we can see, in addition to the heart rate, the ST morphology changes gradually until it recovers its steady state form [38].

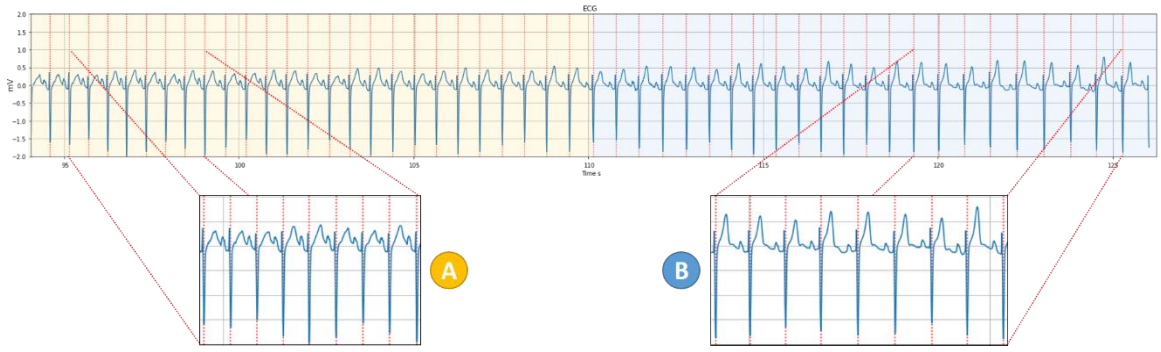

Figure 17. Electrocardiogram recorded after exercise showing two different morphologies, A and B; as we can see, the ST morphology changes gradually until it recovers its steady state.

To solve this issue, we implemented a weighted moving average. We selected a double-sided moving window using five complete cycles at each side to recover the ECG even in heavily corrupted sections. The central R-R section had the highest weight, and the others had a decreasing weight. Using the notation of equation (23), the weighted moving average for a particular R-R section at the instant u will be:

$$\overline{\boldsymbol{y}_u} = \frac{a\boldsymbol{y}_{k_{u-5}}(n) + b\boldsymbol{y}_{k_{u-4}}(n) + c\boldsymbol{y}_{k_{u-3}}(n) + \cdots + f\boldsymbol{y}_{k_u}(n) + \cdots + c\boldsymbol{y}_{k_{u+3}}(n) + b\boldsymbol{y}_{k_{u+4}}(n) + a\boldsymbol{y}_{k_{u+5}}(n)}{2(a+b+c+d+e)+f} \tag{36}$$

With weight factors $a < b < c < d < e < f$=1

Then the complete ECG signal composed of the averaged version of each R-R section after resampling them to their original length will be $\bar{\boldsymbol{x}} = (\bar{\boldsymbol{y}}_u, \bar{\boldsymbol{y}}_{u+1}, \bar{\boldsymbol{y}}_{u+2}, \cdots, \bar{\boldsymbol{y}}_{u+M-5})$.

We can use the averaged version of the ECG as the reference input of an adaptive filter to extract the movement artifacts, as represented in Figure 18; we decided to use the RLS algorithm for this purpose.

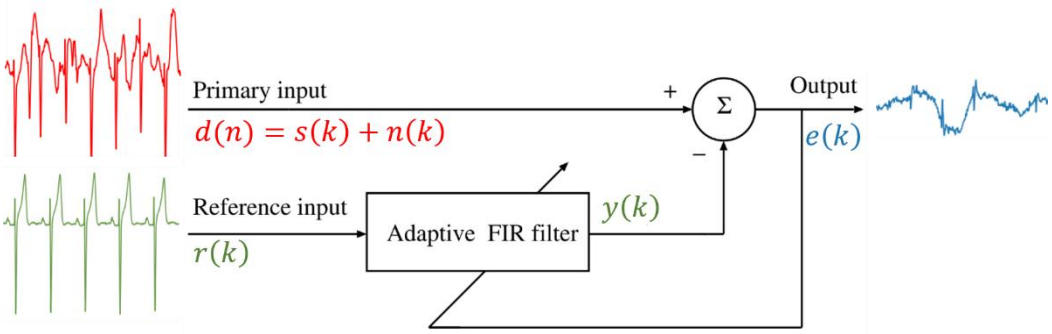

Figure 18. Adaptive filter using the averaged ECG as a reference input to extract noise.

It is worth mentioning that the averaged version of the ECG would cancel all noise sources, including moving artifacts. Then the output of the adaptive filter will be the estimated moving artifacts and additional noise sources.

Finally, with the estimated noise signal, we can calculate the correlation with each component of the IMU and select the best available reference for the adaptive filters.

2.4.2 Wavelet Transform Filter Based on Correlation

A wavelet transform is a linear transformation that decomposes the signal at different resolutions, using a basis function or mother wavelet, utilizing scaling and translations [3]. The transformation can be done in a continuous or a discrete form; the advantage of the discrete form is that it can be computed faster without losing information [46].

A multiresolution wavelet analysis makes it possible to obtain a time-frequency representation of a signal. A key advantage of wavelet techniques is the variety of wavelet functions available. This allows choosing a function whose morphology matches the signal under investigation; for example, in the case of ECG, the Daubechies wavelet family and, in particular, the db6 have a close similarity with the QRS morphology [3]. Multiresolution discrete wavelet transform (DWT) has been applied in ECG and a wide variety of biomedical signals, including Electromyography (EMG), Electroencephalography (EEG), DNA sequences, and respiratory patterns [46].

A discrete wavelet transform (DWT) analyses the signal at multiple resolutions decomposing the signal into successive frequency bands using two sets of functions $\varphi(t)$ and $\psi(t)$ associated with low and high pass filters. These functions can be obtained as the weighted addition of the scaled and shifted version of the wavelet function as follows:

$$\phi(t) = \sum_n h[n]\,\phi(2t - n) \tag{37}$$

$$\psi(t) = \sum_n g[n]\,\phi(2t - n) \tag{38}$$

Where $h[n]$ is the half-band low pass filter, and $g[n]$ is the high pass filter. Then we have the scaling functions $\varphi_{j,k}(t)$ and $\psi_{j,k}(t)$ where j controls the dilation and k the position of the wavelet function.

$$\psi_{j,k}(t) = 2^{-\frac{j}{2}}\psi(2^{-j}t - k) \tag{39}$$

$$\phi_{j,k}(t) = 2^{-\frac{j}{2}}\phi(2^{-j}t - k) \tag{40}$$

With the previous functions, it is possible to obtain different signal frequencies and time localizations utilizing scaling and translations. In addition, successive low and high pass filters of the time domain signal are decomposed into different frequency bands.

At each level of decomposition, the signal is processed with a half-band high pass filter $g[n]$, a low pass filter $h[n]$, and a half-down sampling as follows:

$$D_L[k] = y_{high}[k] = \sum_n x[n] \cdot g(2k - n) \tag{41}$$

$$A_L[k] = y_{low}[k] = \sum_n x[n] \cdot h(2k - n) \tag{42}$$

The output of the high-pass filter $y_{high}[k]$ is the detailed coefficient $D_L$and the output of the low-pass filter $y_{high}[k]$ the approximation coefficient A_L. Successive Decompositions will follow the same procedure; Figure 19 shows the decomposition structure for a 50Hz (Same frequency as the MHEALTH dataset) signal for a decomposition level $L = 7$.

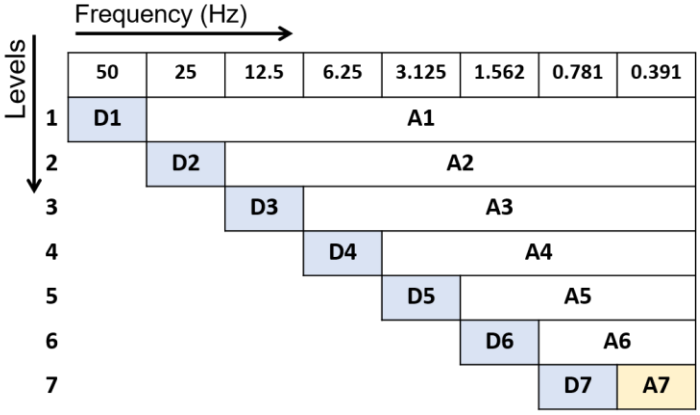

Figure 19. Discrete wavelet transform (DWT) decomposition structure for a 50Hz signal and seven decomposition levels.

After decomposing the signal in the detailed $D_L, D_{L-1}, D_{L-2}, \cdots D_1$ and the approximate band $A_L$we can use the inverse transform to recompose the original signal using the inverse wavelet transform. If we recompose the signal by omitting some levels and setting them to zero (hard thresholding), it would be similar to a block band filter to some extent.

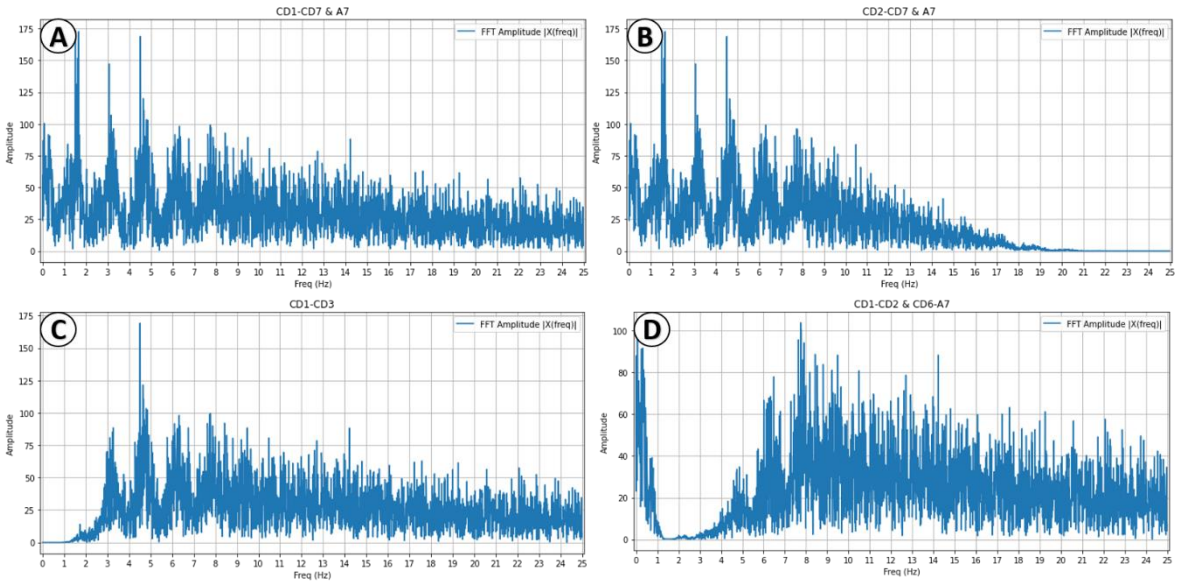

Figure 20. Spectrum diagram of the reconstructed ECG signal omitting different coefficients.

Figure 20 shows an example of the effects on the frequency spectrum after reconstructing an ECG signal recorded at 50Hz from the MHEALTH dataset. The signal was first decomposed into seven levels with a DWT using a "db6" function as the mother wavelet. In Figure 20A, we can see the spectrum without any modification, then in Figure 20B, the effect of removing the first coefficient CD1. Figure 20C shows the effect of removing the low-frequency bands (CD4-A7); lastly, Figure 20D shows the effect of removing CD3, CD4, and CD5.

According to Xiong et al., processing the reference signal with the wavelet transform and removing the wavelet coefficients with low correlation will increase the correlation of the reconstructed signal. As a result, the filter performance would be improved, too [16]. The whole procedure could be synthesized as follows:

1. Select the component from the IMU with the highest correlation per activity.
2. Decomposed the selected component in seven levels ($L = 7$) with a wavelet transform using a "db6" function as the mother wavelet.
3. Calculate the correlation between all the decomposition levels and noise.
4. Recompose the reference omitting the levels with the lowest correlation.

2.4.3 Proposed methodology

As a first step, we processed all data, including the IMU and the ECG components, with a band-pass filter with cutoff frequencies between 0.5Hz and 150Hz.This wot the purpose to keep only the signal inside the spectral range of valuable cardiac information [5], [9], [19], [21], [32], [35], [40]. The following procedure was applied to the MHEALTH dataset and the data recorded with the wearable device:

1. Pre-filter all data (IMU components and the ECG) with a band-pass filter with cutoff frequencies between 0.5 and 150Hz.
2. Identifying R-peaks with an automated algorithm [47].

3. Plot the whole recording, verify if the activities corresponded with the timestamps, and discard the recordings with unacceptable noise.
4. Process the ECG with the weighed synchronized moving average to obtain a clean ECG reference.
5. Extract moving artifacts with an RLS adaptive filter using the WSMA as reference input.
6. Calculate the correlation between the noise extracted in the previous step and the available IMU references. In the case of the MHEALTH dataset, only the 3-axis of the accelerometer was available. On data recorded with Afi, we also included the 3-axis of the gyroscope.
7. Calculate the SNR between the WSMA and the ECG with moving artifacts.
8. Select the component with the highest correlation per activity and use it as the reference input for the LMS, NLS, and RLS adaptive filters.
9. Calculate the ΔSNR of the ECG filtered with the three adaptive filters.
10. Process the component with the highest correlation with the wavelet transform filtering procedure explained previously and calculate the new correlation with the movement artifacts.
11. Use the component processed with the wavelet transform as a reference input for the LMS, NLS, and RLS adaptive filters.
12. Calculate the ΔSNR of the ECG filtered with the three adaptive filters.

3 Results

The following sections describe the experiment's results with the simulated signals and the implemented filters using a reference with different levels of correlation. Then the correlation between isolated movement artifacts and the different axis of the IMUs, and the filter performance using data from the MHEALTH database and recorded with the wearable device AFi.

3.1 Simulated ECG

Figure 21 shows an example of how the LMS, NLMS, and RLS filters perform on a simulated ECG with an SNR=-8.73dB using the same signal as noise and as reference input; as we can see after some iterations, the three filters recovered the original ECG signal to some extent. Nevertheless, the RLS algorithm outperformed the LMS and NLMS regarding convergence speed and ΔSNR.

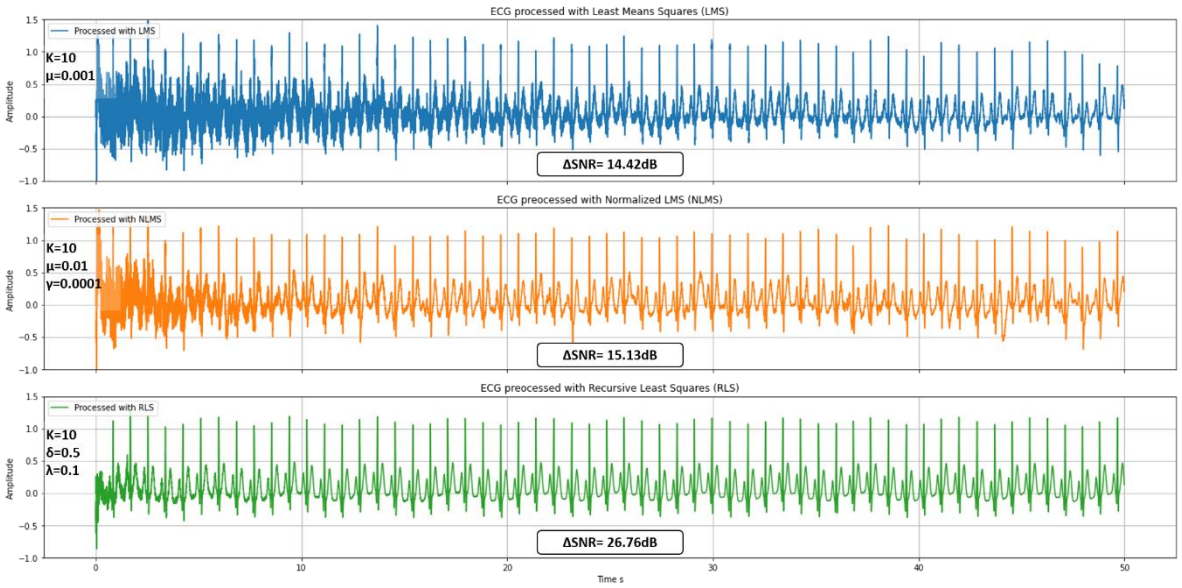

Figure 21. Simulated ECG (SNR=-8.73dB) Figure 12filtered with three 10th order adaptive filters, each graph shows the constants (μ, γ, δ, λ) and the ΔSNR per filter.

LMS and NLMS filters take longer to recover the original ECG signal than the RLS filter; this makes evident the faster convergence of the RLS algorithm (Figure 21). Figure 22 shows how the Root Mean Squared Error (RMSE) calculated for every 64 samples decreases over time to show this effect more clearly. The RLS filter reaches a steady state, with an RMSE close to zero in less than 10 seconds, while with the LMS-based filters, the RMSE decreases at a slower pace but never reaches a steady state. The RMSE was calculated using the same notation as in equation (32) as follows:

$$RMSE = \sqrt{\frac{1}{N}\sum_{n=1}^{N}[x(n) - \tilde{x}(n)]^2} \tag{43}$$

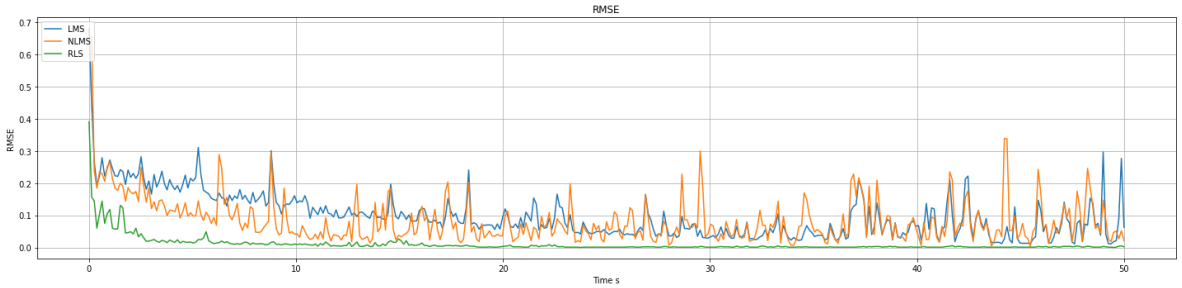

Figure 22. Root Mean Squared Error (RMSE) behavior over time of LMS, NLMS, and RLS filters calculated on windows of 64 samples.

To show how the filters behave with different correlation values, we decreased the correlation from ρ=1 to ρ=0.8, ρ=0.4, ρ=0.2, and ρ=0.1 by adding every time more random noise to the reference. Table 1 shows the results after performing the same experiments 50 times; the first row shows the Pearson correlation between the reference signal and noise. The second row is the mean SNR of the noisy ECG, followed by the mean ΔSNR after filtering the signal with the three filters.

The first column per correlation shows the ΔSNR of the complete signal (100%), and the second column is the ΔSNR of the second half of the signal (50%) to avoid the adaptation phase[8]. As the correlation decreases, the performance of the three filters decreases; this is evident with lower ΔSNR. When the correlation is as low as ρ=0.1, the filter could add noise instead of reducing it; we can see this effect with the negative ΔSNR shown in red in Table 1.

Table 1. Mean ΔSNR in dB after applying three adaptive filters to a simulated ECG signal corrupted with noise; the experiment was repeated 50 times per correlation value (ρ=1 to ρ=0.1).

Correlation	ρ = 1		ρ = 0.8		ρ = 0.4		ρ = 0.2		ρ=0.1	
ECG + Noise (SNR)	-6.78		-7.37		-6.85		-6.32		-6.43	
	100%	+50%	100%	+50%	100%	+50%	100%	+50%	100%	+50%
LMS (ΔSNR)	15.36	12.37	8.92	11.81	4.06	7.72	2.01	5.9	-0.42	5.27
NLMS (ΔSNR)	8.91	7.43	8.73	10.81	4.06	7.47	1.71	5.65	-0.47	5.1
RLS (ΔSNR)	23.85	25.71	9.81	21.29	4.22	9.98	1.65	7.36	0.46	6.58

From Table 1, we can conclude that with high correlation values above ρ=0.8, the RLS filter has a remarkably superior performance with ΔSNR at least two times higher than the LMS-based filters. The difference between the three filters is not as significant with lower correlations. It is worth noting that the morphology recovery is negligible with a reference with a low correlation. Figure 23 shows an ECG signal after being processed with three adaptive filters and a reference signal with different correlation values ρ=0.8, ρ=0.4, and ρ=0.1; the figure also shows the raw, noisy signal with added noise of -6.84dB before being filtered.

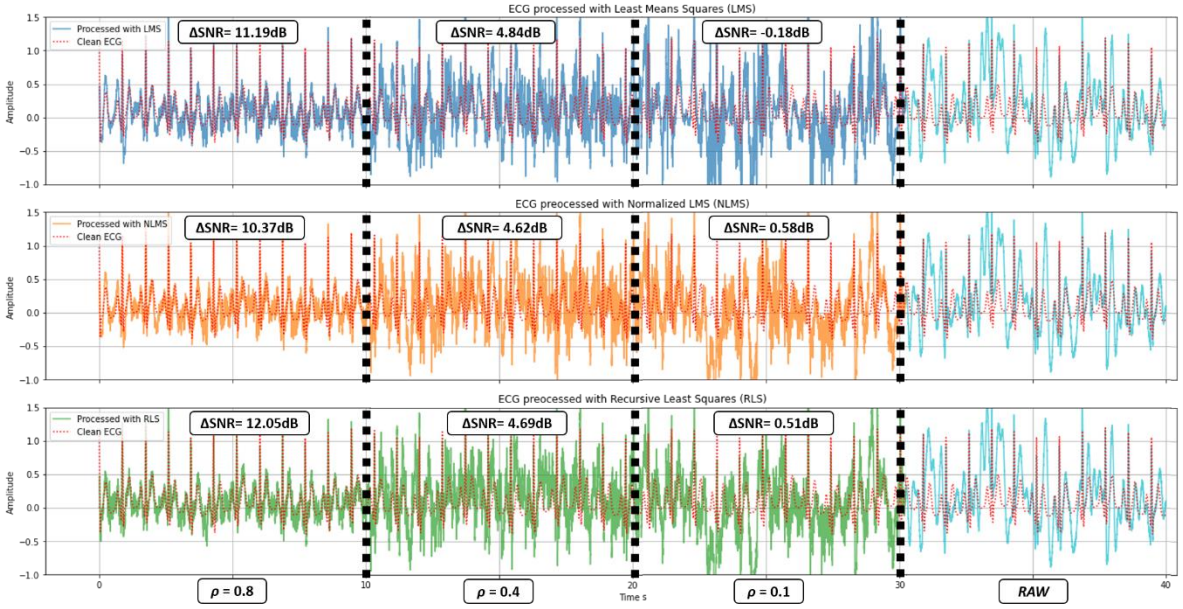

Figure 23 Noisy ECG signal (-6.84dB) after being processed with three adaptive filters and a reference signal with different correlation values.

From Figure 23, we can see that only with a correlation of ρ=0.8 the morphology of the ECG was partially recovered, the R peaks are clearly identifiable, and even though the signal still has a significant amount of noise, it follows the red dotted line that represents the clean ECG. With correlation values below 0.8, the morphology

[8] We defined the adaptation phase as the time it take the filter coefficients $\boldsymbol{w}(k)$, to transition from the initialization value usually set to zero $\boldsymbol{w}(0) = [w_0 = 0, w_1 = 0, \cdots w_N = 0]^T$ to the appropriate range of values depending on data, and the update coefficient equation.

recovery is negligible; with ρ=0.4, some R peaks coincide with the red dotted line, but they could be easily confused with all the other spikes. Figure 23 gives us an idea of the negative effect of adaptive filters using a reference with low correlation.

3.2 Online and Recorded ECG

This section will show the complete procedure in detail with an example from one of the activities. The same procedure was repeated on the five activities of the eight recordings made with the wearable device AFi and the five recordings and four activities from different subjects from the MHEALTH database.

One of the restrictions of the WSMA is that it relies on the correct identification of R-peaks; for this reason and consistency, we had to exclude some intervals where the noise level impeded the automated algorithm from detecting the R-peaks correctly. We also excluded regions with significant flat lines. Figure 24 shows two examples of regions we had to discard with unacceptable noise levels.

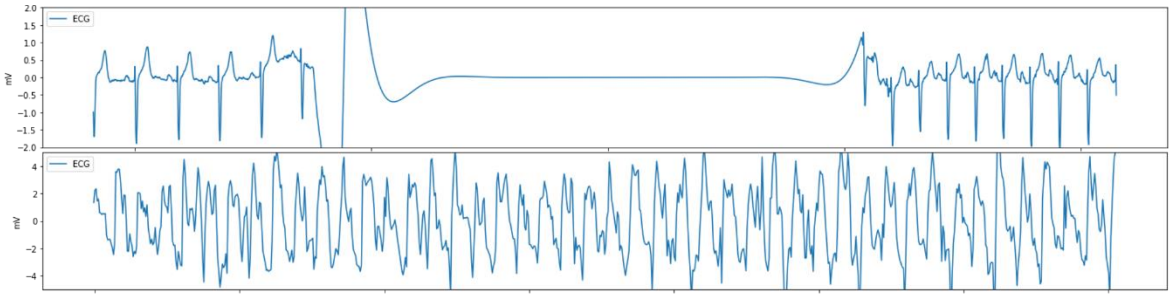

Figure 24. Two kinds of unacceptable noises. In the top graph, a flat line appears due to device saturation, and in the second, the amount of noise impedes the automatic algorithm from identifying the r-peaks correctly.

Figure 25 shows the result of the first three steps of the proposed methodology. The top graph shows the pre-filtered ECG with moving artifacts and the R-peaks identified by the automatic algorithm. The second graph shows the 3-axis of the accelerometer, and the third one is the 3-axis of the gyroscope; as this recording was taken while the participant was jumping, the high amplitude peaks of the vertical axis or x-axis of the accelerometer make evident every single jump. As the R-peaks were correctly identified, the recording was considered to have an acceptable amount of noise.

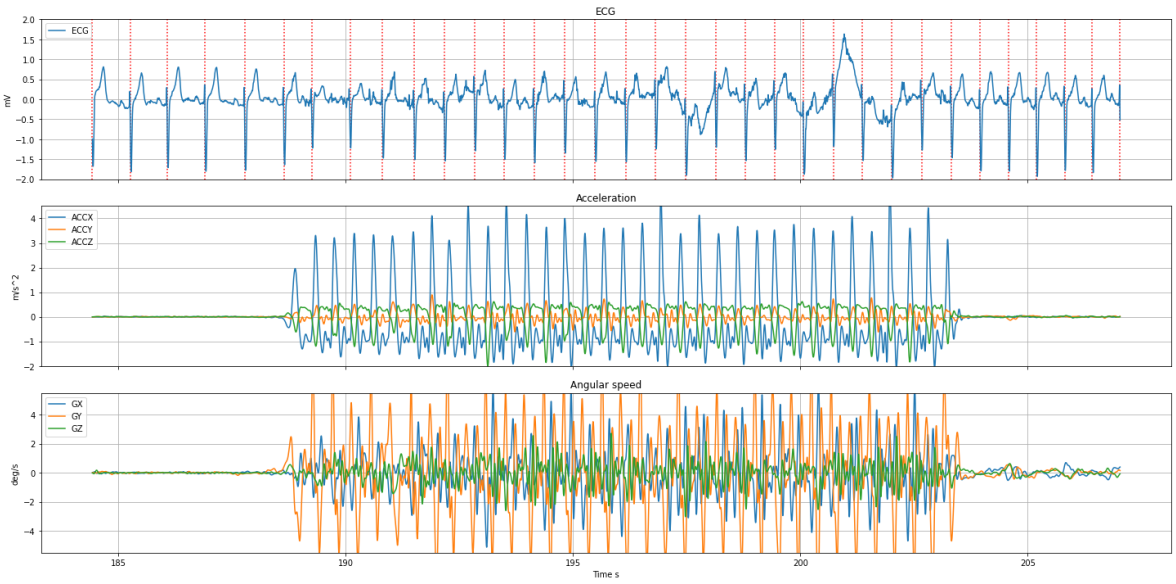

Figure 25. Data recorded with the wearable device AFi, the first graph shows the ECG, the second the 3-axis of the accelerometer, and the third one the 3-axis of the gyroscope.

Once verified that the R-peaks were identified, the next steps (4-7) are shown in Figure 26. In the middle graph, we can see the WSMA of the original ECG, and then in the last graph, the movement artifacts extracted with the RLS adaptive filter. The signal-to-noise ratio calculated between the WSMA and ECG with moving artifacts is 5.55 dB which is not significant considering the intensity of the physical activity.

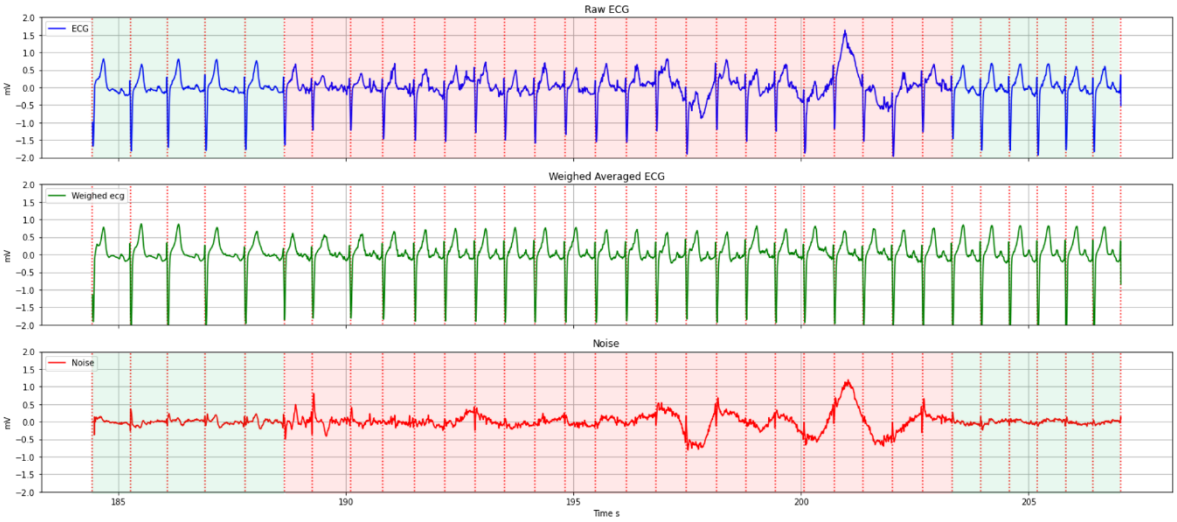

Figure 26. The first graph shows the ECG with movement artifacts, the second the weighed synchronized moving average, and the third graph shows the noise extracted with the RLS filter.

Afterward, we calculated the Pearson correlation between the noise extracted with the RLS filter and the different components of the IMU, as shown in TABLE 2. And as we can see, the component with the highest correlation GY that corresponds to the y-axis of the gyroscope was used as the reference input for the adaptive filters. We also calculated the correlation between the different components and the ECG with moving artifacts. As we can see, the correlation is even smaller, and the maximum values were not coincident.

Table 2. Absolut Pearson correlation between the different components of the IMU and the noise extracted with the RLS filter and with the ECG with movement artifacts.

	ACCX	ACCY	ACCZ	GX	GY	GZ	AVM
Noise	0.046	0.019	0.050	0.064	0.078	0.051	0.049
ECG	0.006	0.003	0.019	0.053	0.013	0.045	0.029

Figure 27 shows how the filters behaved using GY as a reference input; we also plotted the original unfiltered ECG with a red dotted line to show how the filter modified the signal. As we can see, the LMS filter presented several instability problems decreasing the amplitude of the S-peaks. The NLMS corrupted, even more, the original signal, especially at the start of the noisy region. The RLS also had some stability issues at the beginning of the noisy region, but overall, it affected the original signal; nevertheless, it did not improve it either. The three filters showed negative ΔSNR, which means that the filtering process added more noise to the original signal, which was expected according to the experiments with the simulated signal due to the low correlation.

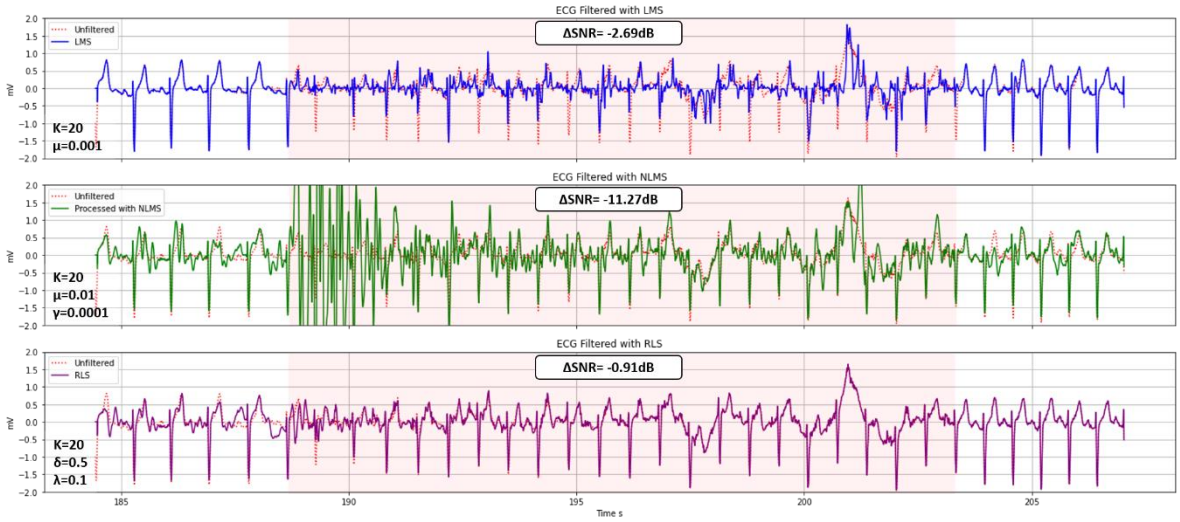

Figure 27. Adaptive filters using the Y axis of the gyroscope as reference input.

Subsequently, we tried to improve the correlation by filtering the reference; for this, we applied a 6th-order wavelet transform using a 'db6' as the mother wavelet and calculated the correlation between the wavelet coefficients and noise, as shown in FIGURE 28. According to the method proposed by Xiong et al. (2020) [16] we selected the coefficients with the lowest correlation, set them to zero, and recomposed the reference signal with the remaining coefficients. Afterward, we calculated the correlation between the reconstructed reference and noise correlation increased from ρ=0.078 to ρ=0.087.

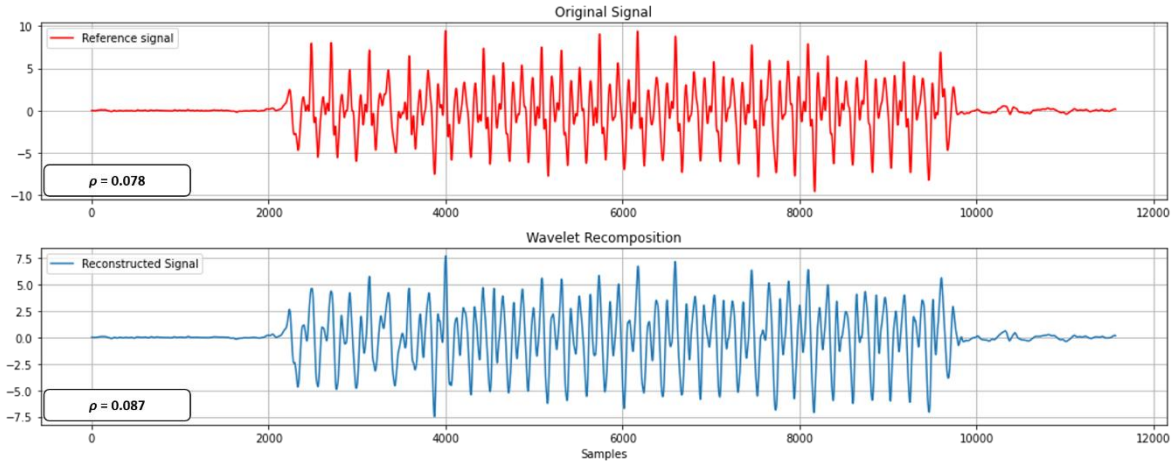

Coefficients	cD1	cD2	cD3	cD4	cD5	cD6	cA6
Noise	ρ = 0.001	ρ = 0.001	ρ = 0.010	ρ = 0.001	ρ = 0.021	ρ = 0.020	ρ = 0.028

Figure 28. Original reference (GY) and after processed with a wavelet transform, both with their corresponding correlation. The table below shows the correlation between the wavelet coefficients and noise, the coefficients in red were set to zero before reconstructing the signal.

Then we tested the filters again using the reconstructed component (GY) as reference input. Because the increase in correlation was negligible, the LMS and RLS filters behaved almost the same. In the NLMS filter, the instability effect that appeared at the beginning of the noise section, this time, got boosted, burying the ECG signal completely.

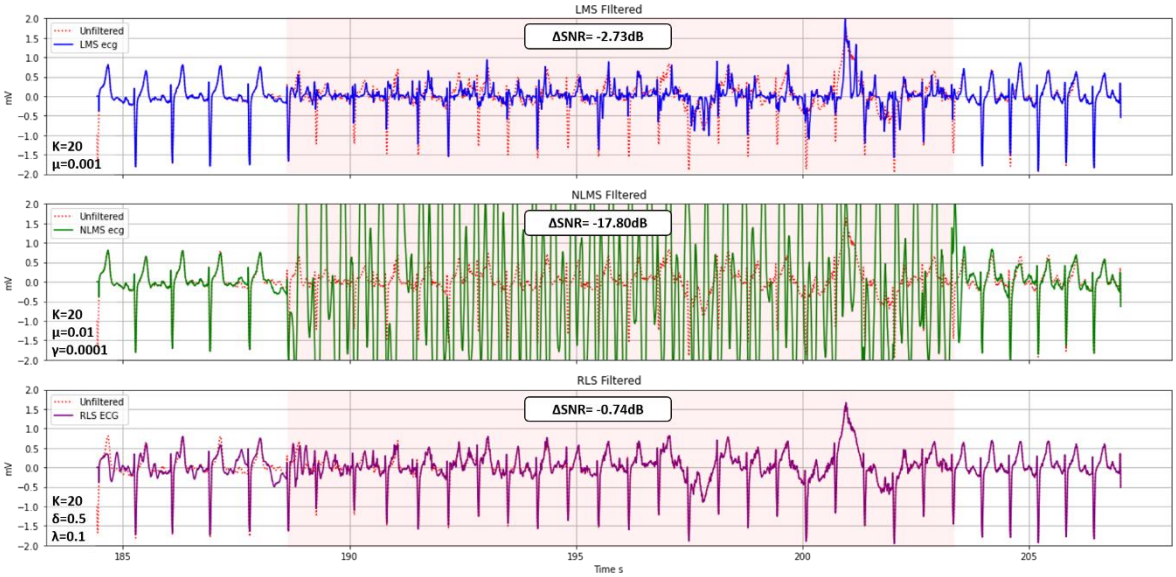

Figure 29. Adaptive filters use the reconstructed reference signal as reference input.

In most cases, the filters behaved as in the previous example due to low correlation. Figure 30 shows the filter output of a particular case corresponding to the highest correlation registered from our experiments $\rho = 0.554$. With such correlation the LMS and the RLS slightly improved the original signal in terms of ΔSNR. However, if we take a closer look at Figure 30, there were some points where the filter introduced artifacts in the form of steep peaks to the original signal. The artifacts were evident on the NLMS through the whole noisy section (red zone) and at the initial part of the noisy section with the RLS filter.

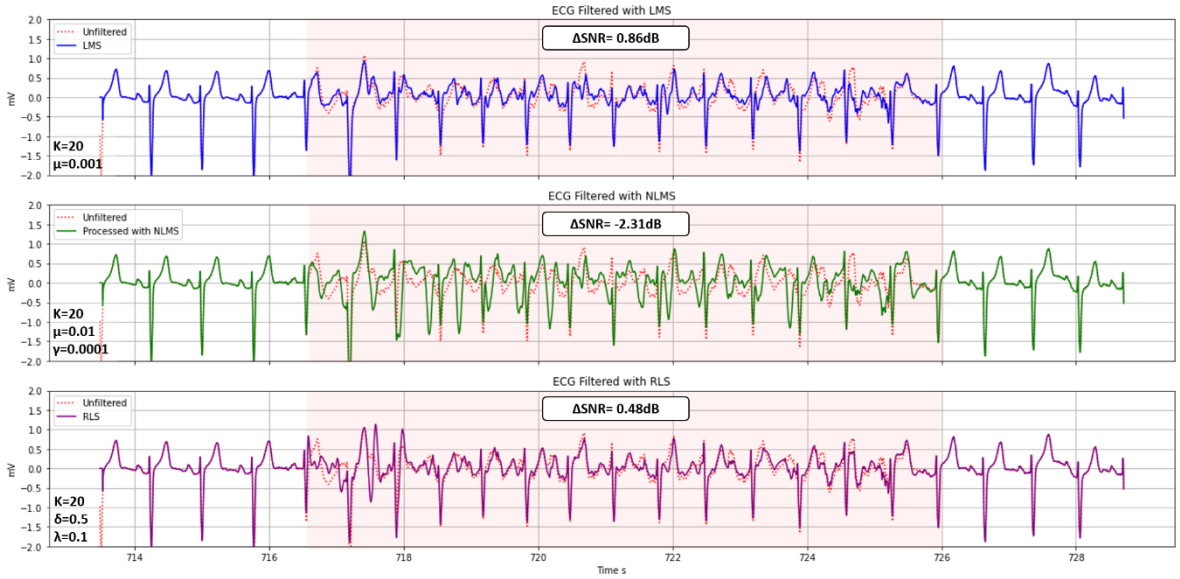

Figure 30. ECG processed with the LMS, NLMS, and RLS adaptive filters, using the z-axis as reference input. The red zone indicates the starting and ending point of the noisy section.

Applying the wavelet decomposition method to the z-axis, the correlation between the movement artifacts and the recomposed z-axis increases to $\rho = 0.635$. Using the recomposed signal as a reference input for the AFs, the ΔSNR increases slightly compared to the ΔSNR using the original z-axis. Still, as shown in Figure 31, the adaptive filters introduced artifacts to the original signal.

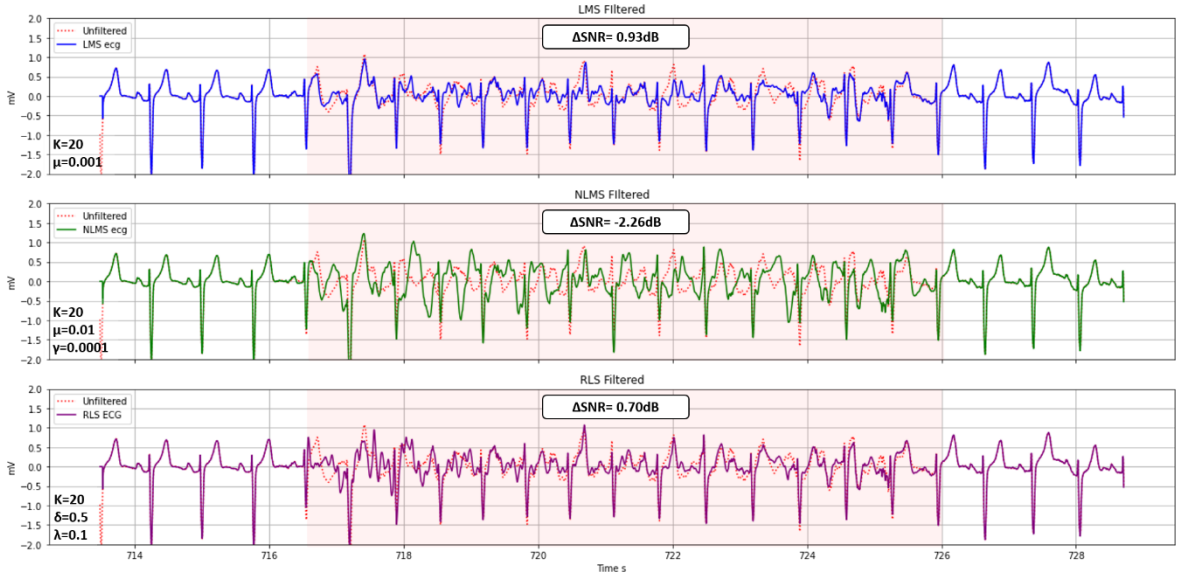

Figure 31. Filter output using the recomposed reference input after being processed with the wavelet transform method.

As we have seen with the last example, even with the highest correlation we found in our experiments, none of the filters significantly improved the ECG signal quality. Moreover, as we will describe in the following section, the correlation value from this example was an outlier, as most of the values were much smaller.

3.2.1 Correlation

In this section, we will analyze the correlation values depending on the physical activity and the different axis of the IMU from the MHEALTH dataset and data recorded with AFi. The results are displayed in several boxplots to see the data distribution; we used the same scale to make the comparison easier. In all cases, the blue color represented the x-axis that coincides with the vertical axis, the orange color the y-axis, the green color z-axis, and the cyan color the acceleration vector magnitude. In every boxplot, the red diamond shows the mean value, and the horizontal line is the median per axis.

Figure 32 shows the correlation between the movement artifacts and the different components of the IMU recorded with the wearable device AFi. As we can see, the correlation coefficients were generally very low, with some outliers above 0.2. Additionally, there was not a big difference between activities with high (running, jumping), low intensity (walking), and activities without displacement (pushups, torso rotations). It is worth noting that the mean SNR values per physical activity recorded were generally quite high, meaning that the physical activities did not produce a significant amount of movement artifacts. The pushups had the lowest mean SNR; however, the recordings were corrupted with electromyography noise from the pectoral muscles, which is not, by definition, a movement artifact.

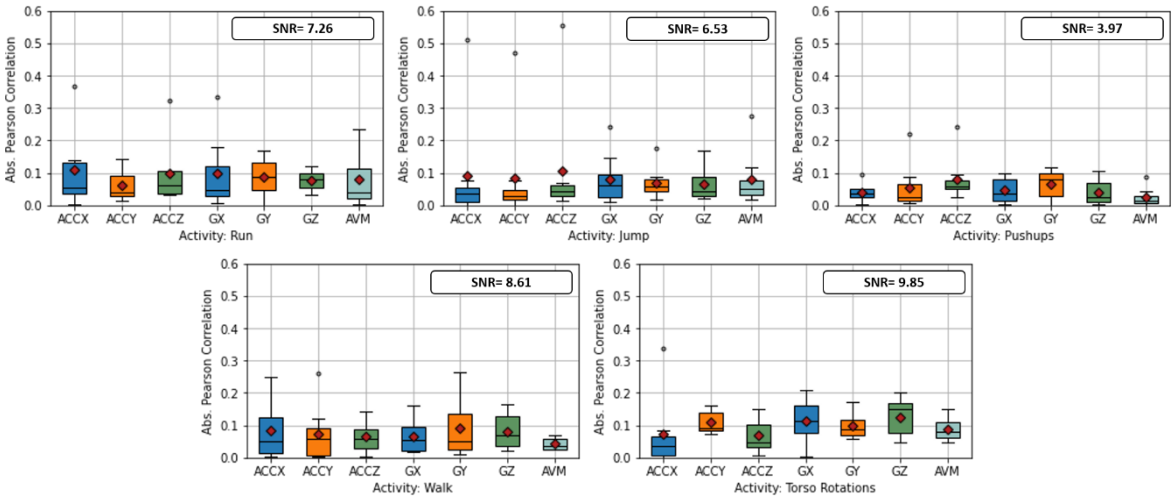

Figure 32. Box plots showing the absolute value of the Pearson correlation between movement artifacts and the components of the IMU per activity for the data recorded with the wearable device.

The following figure shows the Pearson correlation per activity, this time with data from the MHEALTH dataset. The values were comparable with the data recorded with the wearable device, with no significant difference between high-intensity activities (running, jumping) and low-intensity (walking) and with no translation (squats).

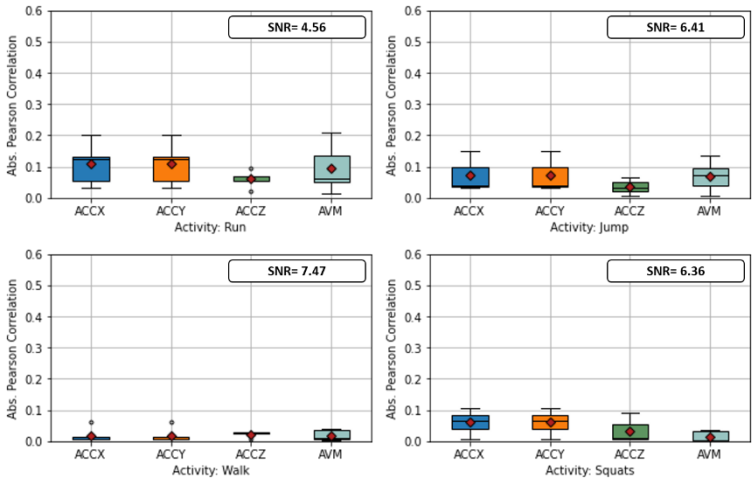

Figure 33. Boxplots showing the absolute value of the Pearson correlation between movement artifacts and the components of the IMU per activity from the MHEALTH dataset.

Figure 34 shows the values combined from all the activities. To find if there was a component with higher correlations than the others, regardless of the activity. Nevertheless, none of the components showed to be above the others.

Taking a closer look at Figure 34A, the third quartile represented by the top border of the colored boxes from all axis was around 0.1, meaning that 75% of the values were below this line. Comparing the accelerometer and the gyroscope correlations, the accelerometer axis had more outliers above 0.2, but the top whiskers of the gyroscope axis extended slightly above the accelerometer boxplot whiskers, which means that 25% of the top values were between 0.1 and around 0.2. The median values were around the same range between 0.05 and 0.1, and the mean values of the accelerometers were higher due to the number of outliers.

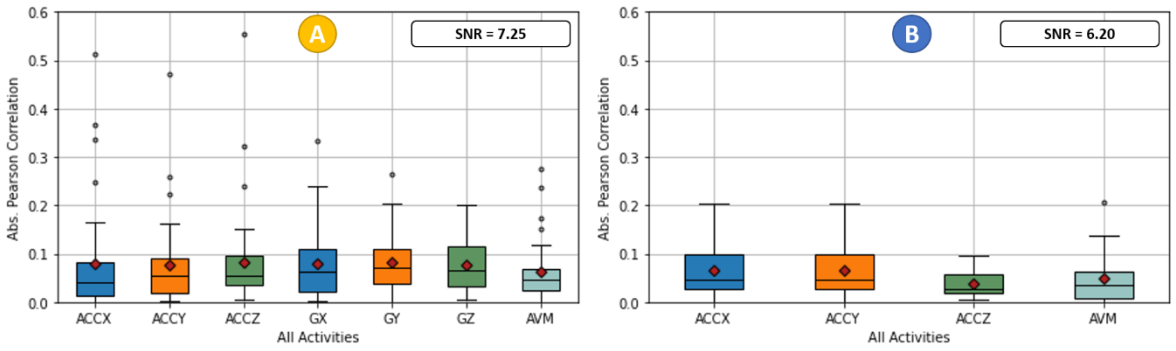

Figure 34. Absolute Pearson correlation value per IMU component. Figure A shows data recorded with the wearable device, and figure B shows data from the MHEALTH dataset.

On data from the MHEALTH dataset (Figure 34B), the top whiskers extended from 0.1 to around 0.2 in the case of the x-axis and y-axis of the accelerometer; this is higher than the data recorded with the wearable device AFi. The whole distribution of the z-axis was below the third quartile of the other two axes, meaning that the z-axis (perpendicular to the body) had the lowest correlation coefficients.

3.2.2 Filter Performance

The filter performance was heavily affected by the low correlation values. TABLE 3 first shows the ΔSNR after applying the adaptive filters to ECG recorded with the wearable device AFi. As we can see, all values are negative, which means that the filters introduced more noise to the original signal. The same table shows the filter performance after applying the wavelet transform method to the reference with the highest correlation. As we can see, on average, the values remained almost the same. The change in correlation after applying the wavelet transform filter was insignificant in most cases, and in many cases, it remained the same or slightly reduced. On average, the change in correlation using the reference processed with the wavelet transform was $\Delta\rho$=-0.014.

Table 3. Filter performance on average per activity in ΔSNR before and after processing the reference input with the wavelet transform using data from the WD Afi.

	SNR	Max ρ	ΔSNR LMS	ΔSNR NLMS	ΔSNR RLS	New ρ	ΔSNR LMS	ΔSNR NLMS	ΔSNR RLS	$\Delta\rho$
Jumping	6.53	0.254	-26.627	-2.357	-0.320	0.259	-24.956	-2.893	-0.240	0.005
Torso Rotation	9.85	0.191	-4.240	-0.407	-0.836	0.192	-4.244	-0.081	-0.819	0.001
Pushups	3.97	0.113	-2.709	-0.556	-0.133	0.113	-2.711	-0.084	-0.137	0.000
Walk	8.61	0.148	-3.550	-1.626	-0.897	0.106	-3.471	-0.041	-0.840	-0.043
Run	7.26	0.159	-42.630	-0.241	-0.824	0.127	-13.201	-0.024	-0.703	-0.032
Average	**7.25**	**0.173**	**-15.951**	**-1.037**	**-0.602**	**0.159**	**-9.717**	**-0.625**	**-0.548**	**-0.014**

In some cases, the LMS filter buried the signal completely in noise; we can see this in the table with the highly negative ΔSNR values. On the other hand, the NLMS and the RLS maintained the signal almost unchanged in terms of SNR. On average filtering, the reference signal with the wavelet transform increased the ΔSNR; nevertheless, the effect was almost negligible.

Table 4. Filter performance on average per activity in ΔSNR before and after processing the reference input with the wavelet transform using data from the MHEALTH database.

	SNR	Max ρ	ΔSNR LMS	ΔSNR NLMS	ΔSNR RLS	New ρ	ΔSNR LMS	ΔSNR NLMS	ΔSNR RLS	$\Delta\rho$
Jumping	6.41	0.126	-2.760	-0.088	-1.432	-0.048	-1.882	-0.090	-2.198	-0.174
Squats	6.36	0.087	0.024	-0.020	-0.678	0.039	-0.012	-0.026	-0.686	-0.048
Walk	7.47	0.076	-0.088	-0.026	-0.740	0.029	-0.078	-0.026	-0.600	-0.047
Run	4.56	0.107	-1.456	-0.030	-1.066	0.066	-0.646	-0.036	-0.960	-0.041
Average	**6.20**	**0.099**	**-1.070**	**-0.041**	**-0.979**	**0.021**	**-0.655**	**-0.044**	**-1.111**	**-0.078**

As we can see from Table 4, the filter performance of the LMS, NLMS, and RLS with data from the MHEALTH dataset was similar to data recorded with the WD Afi. The only relevant difference was that the LMS did not corrupt the original signal as much as in the experiments with the WD.

4 Discussions

From the experiments with the simulated signals, we could see that the RLS filter has superior performance than LMS-based filters in terms of convergence speed and minimization of the RMSE. Even when the signal was highly corrupted with noise (SNR≈-10), the RLS was able to recover the ECG given a reference input with enough correlation with the noise source (ρ>0.8).

Moreover, the experiments with simulated signals showed us the negative effects of using a reference input with low correlation, regardless of the adaptive filter used. In this scenario, instead of recovering the original ECG morphology, the adaptive filters added artifacts to the filtered signal. These artifacts had a similar shape to the reference; as we can see in Figure 35, the filtered signal with the RLS resembled the peaks of the random noise from the reference signal. This same behavior was observed in the experiments with real ECG data.

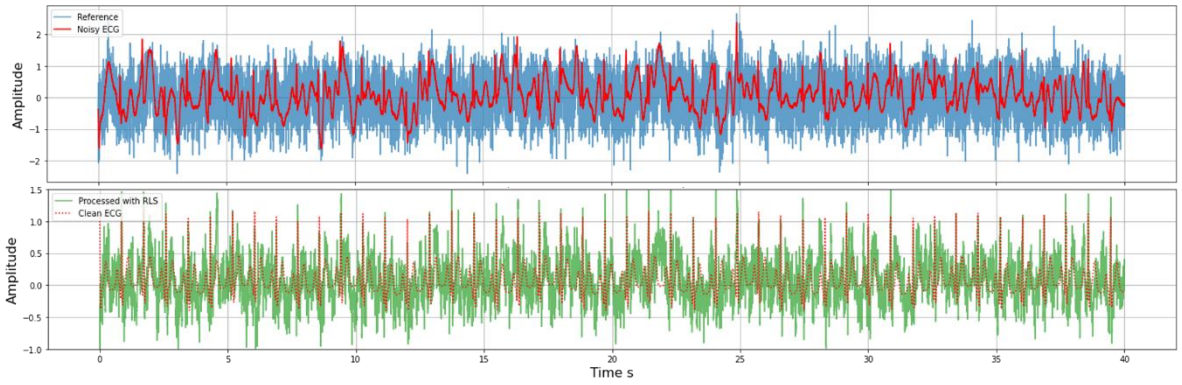

Figure 35. Top) Simulated ECG corrupted with noise with an SNR -6.65dB and the reference signal with a correlation of ρ=0.4. Down) Clean ECG and after processed with an RLS filter ΔSNR= 4.52.

Figure 36 shows the same recording as in Figure 30, and the reference signal is the accelerometer's z-axis with a correlation of ρ=0.554. The top graph shows the output of the NLMS filter (blue line); as we can see, the filter modified the original signal (red dotted line), introducing additional artifacts that followed the shape of the reference signal (green signal). The RLS filter suffered a similar effect at the beginning of the noisy region (yellow zone); nonetheless, the RLS filter reacted faster and preserved the ECG without introducing additional artifacts. Adaptive filters update their coefficient vector following the reference input and output error; for this reason, low-correlated references could affect the filter output instead of improving the filter's signal. Nevertheless, we have seen that the RLS filter was less susceptible than the LMS-based filters to low-correlated references.

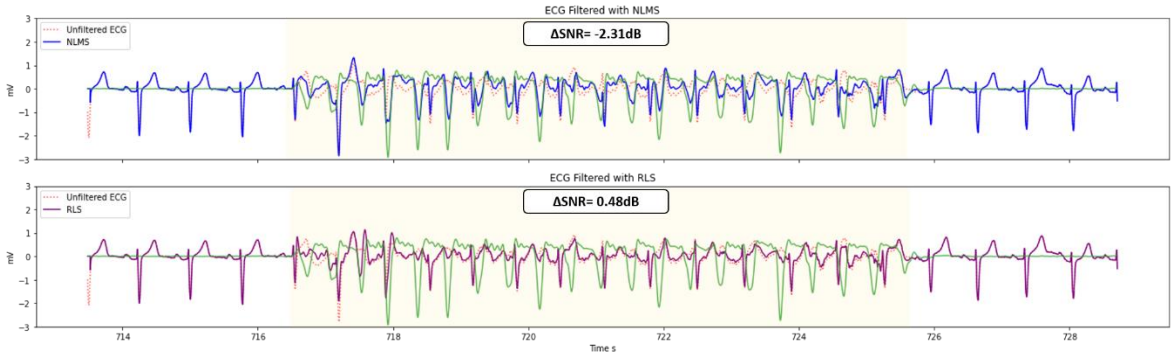

Figure 36. The top figure shows the output of a NLMS and the bottom of an RLS filter from the same ECG signal; in both, the reference input corresponds to the z-axis of the accelerometer shown in green.

In combination with the RLS filter, the weighed synchronized averaged method offers a feasible alternative to extract a rough estimation of the noise superimposed to the ECG signal in scenarios where a clean ECG is unavailable. Nevertheless, it requires the correct identification and location of the R-peaks, restricting its use to ECG recordings where automatic QRS detection algorithms can still locate the R-peaks. However, the noise extracted with the RLS filter includes all noise sources, whether they are movement artifacts. Moreover, individual differences between heartbeats will be extracted as noise, evident as small spikes at the location of the R-peaks.

Figure 37 shows an ECG recorded while the subject was doing several pushups; as we can see, the recording is corrupted with both moving artifacts and electromyography noise from the pectoral muscles. The same figure shows the rough estimation of noise extracted with the WSMA and an RLS filter; as we can see, it includes the EMG noise recognizable as high-frequency spikes. Something worth noting is that at the beginning and the end of the noise region (red zone), the ECG is corrupted only with MA that appeared due to the transition from a vertical to a horizontal position for doing the pushups.

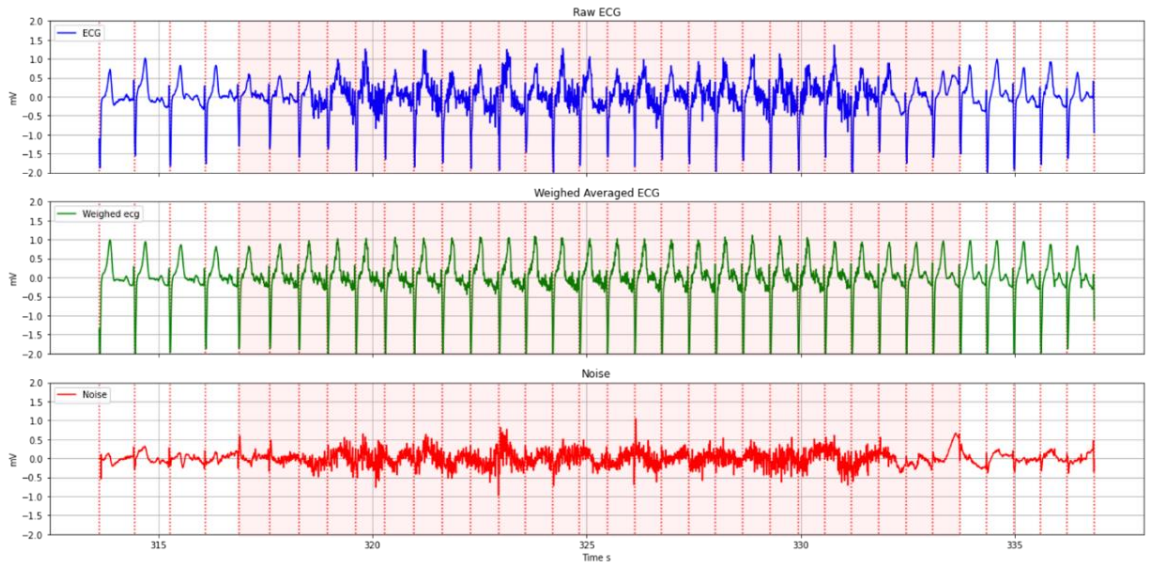

Figure 37. The top figure shows an ECG recorded while the subject was doing pushups, the middle shows the WSMA, and the third is the noise extracted with an RLS filter, including moving artifacts and EMG noise.

Moreover, using the WSMA could provide an objective rough estimation of the noise level when a clean ECG reference is unavailable, as in the case of a single lead ECG recorded with a wearable device. Calculating the SNR between the ECG signal and the WSMA would be a fair estimation of how much each R-R interval deviates from the average calculated using adjacent heartbeats. Figure 38 shows two examples; the left one with a higher amount of noise than the right one and the corresponding SNR per signal. Nevertheless, this method must be tested extensively and with more data.

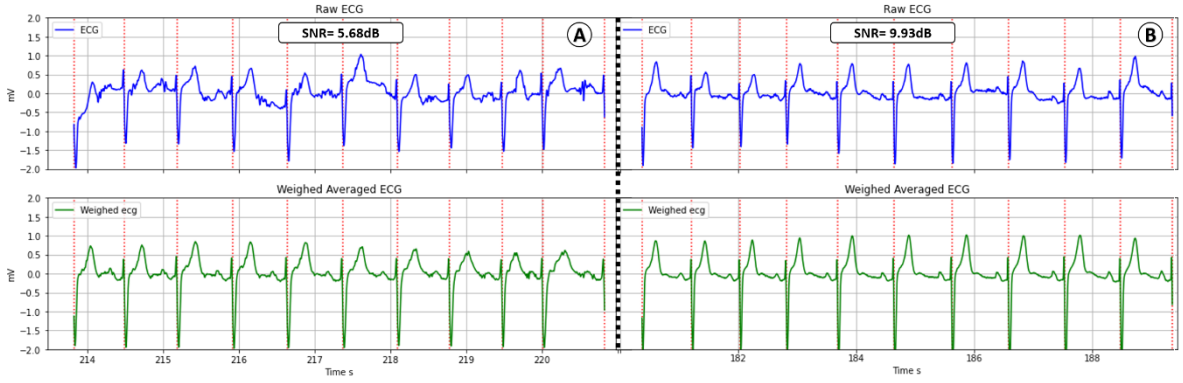

Figure 38. SNR calculated using the WSMA, and the original signal, the left graphs (A) show the example of a noisy region, and the right graphs (B) show a cleaner region.

IMU data recorded with the wearable device and dat from the online database showed very low correlation values with movement artifacts. Consequently, when we used the components as reference inputs for the different adaptive filters, they all showed very poor results, usually adding more noise to the original signal.

Martini et al. [9] reported correlations above ρ=0.6 and up to ρ=0.9 using 3 seconds time windows; they also considered values with a time lag up to 1s. Additionally, their experimental setup was different as they induced movement artifacts by hand on one electrode while using the other as a reference on a 2-lead ECG recorded at

rest. Lilienthal et al. (2021) also reported higher correlation values up to ρ=0.45 without considering outliers. They calculated the correlation with a moving window (The window size was not specified) and in different time lags up to 1s [19] Also, Xiong et al. (2020) reported higher correlation values between ρ=0.2 and ρ=0.54. However, they recorded ECG with fabric electrodes that are more prone to suffer from movement artifacts than Ag/AgCl electrodes [16].

Something important to note is that a correlation coefficient is a statistical value that describes the strength of the linear association between two variables through the observation interval. If the observation interval is not representative, the conclusions drawn would not be meaningful [20].

We calculated the correlation per activity, assuming that the repetitive movements would generate consistent, repetitive artifacts. Nevertheless, the artifacts were not consistent. Smaller time windows might show higher correlation values capturing instants where the different IMU components and MA match even by chance. Calculating the correlation in smaller time windows and constantly switching between the reference signals choosing the one with the highest correlation per window could be an alternative. However, the abrupt changes between the references may lead to instability problems with the adaptive filters; this remains an open question.

Additionally, the ECG recorded with Afi was not heavily affected by movement artifacts; even with high-intensity activities, the mean SNR was 7.26dB for running and 6.53dB for jumping. While for low-intensity activities, the mean SNR was 8.61dB for walking and 9.85dB for torso rotations. The lowest mean SNR was registered with pushups (3.97dB), but in this case, the main source was EMG noise and not movement artifacts.

The low incidence of movement artifacts could be the main reason for the low correlation values. While the accelerometer and the gyroscope registered intense body movements, in most cases, the ECG was affected by low amplitude artifacts and sporadic baseline shifts. We can see three examples in Figure 39; the noise extracted from the ECG did not match the repetitive variations registered by the IMU references.

From all the recordings (R1-R8) with the WD Afi, only three activities were discarded after significant flat lines (torso rotations, pushups, and running), and all were from the same recording (R1). Additionally, almost all the high correlation outliers were from a different recording (R8). The different behavior of recordings R1 and R8 could be related to factors that changed per recording, such as skin preparation.

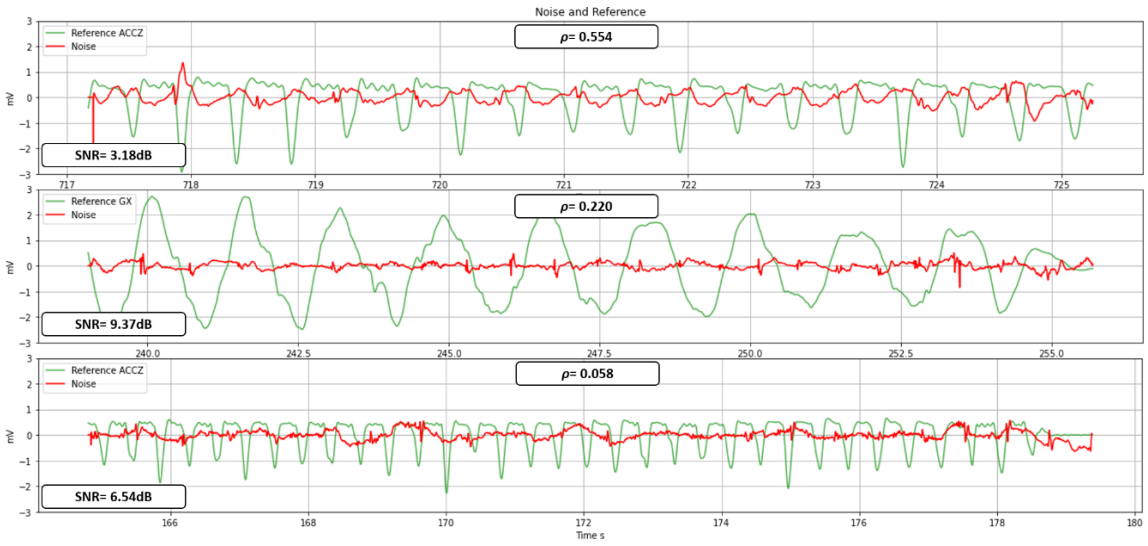

Figure 39. Three examples with different correlation values, the red line is the noise extracted from ECG recorded with the WD Afi, and the green line is the IMU axis with the highest correlation.

On the other hand, the wavelet filtering method applied to the IMU components showed, on average, no improvement in the correlation. This could have been due to the correlation values being very low, and Xiong et al. (2020) [16] reported correlation improvements with his method with signals above 0.2. The few outliers with correlation values above 0.2 showed negligible correlation improvements in our experiments.

While correlation coefficients $\rho<0.1$ indicate a negligible correlation and $\rho>0.9$, very strong relationship values in between are debatable [20]. For this reason, small changes in correlation would not be significant because samples are inevitably affected by chance.

Adaptive filters need a reference that correlates with movement artifacts continuously and not only sporadically, a reference signal that would be able to predict, to some extent, the fluctuations of noise. Adaptive filters have been successfully implemented in applications with a reliable correlated reference. For example, for filtering the maternal ECG from the fetal ECG recorded with an abdominal lead, in this example, the reference input is the maternal ECG recorded from the chest [17].

5 Conclusions

With the simulated signals experiments, the RLS filter showed superior performance than the LMS-based filters in terms of convergence speed and minimization of the RMSE. Nevertheless, it requires a high correlation between the reference input and the undesired signal or noise to provide a proper signal enhancement and morphology recovery.

The low correlation between MA and the different axis of the IMU sensors from data recorded with the wearable device Afi and data from the MHEALTH dataset affected the performance of the LMS, NLMS, and RLS filters. On data recorded with the WD Afi, the NLMS and RLS were less susceptible to adverse effects when using a reference input with low correlation than the LMS filter. All filters behaved comparably on data from the MHEALTH dataset with a low correlation reference input. Moreover, on average, the wavelet transform method for preprocessing the reference input showed negligible effects in both correlation and filter performance, possibly after low correlation.

The low incidence of movement artifacts could be the main reason for the low correlation values. While the accelerometer and the gyroscope registered intense body movements, the ECG was affected by low amplitude artifacts and sporadic baseline shifts in most cases. For the reasons above, the correlation between motion artifacts and body movements recorded with inertial sensors appeared to be low and inconsistent. Given this, adaptive filters using inertial sensors as reference input are unsuitable for removing ECG movement artifacts in recordings with low noise levels.

The RLS could be an alternative only in settings where skin preparation is not possible or with ECG recorded with fabric electrodes more prone to movement artifacts, but only if a reference with higher correlation is available. Direct skin resistance measurement could be a possible candidate. This remains an open question and future work.

6 Acknowledgments

I'm incredibly grateful to my family and especially to my mother, Eugenia Ramirez, my father, Cesar Cornejo, and my brother Daniel Cornejo for their unconditional support in all my adventures and challenges.

I want to extend my sincere thanks to my supervisors, Borbala Hunyadi and Pourya Omidi, for trusting me and giving me their invaluable guidance throughout the project.

I am also grateful to my friends Anna Graell, Cristina Cretu, Edwin Tay, Flora Guarnotta, Gabriel Turcan, Kristyna Herman, Davashish Mantri, Max Cortes, Mauricio Saldivar, and Rebecca Breda for being part of the journey and being like my family in this two years.

Many thanks to my colleagues from Praxa Sense for introducing me to the Dutch culture and for their assistance during the project.

And special thanks to Martina Cuschieri for her invaluable assistance.

7 References

[1] E. N. Marieb and K. N. Hoehn, *Human Anatomy & Physiology, Global Edition*, vol. Tenth Edition. Pearson Education Limited, 2019.

[2] R. M. Rangayyan, *Biomedical Signal Analysis*, Second Edition. New Jersey: John Wiley & Sons, Inc., 2015.

[3] S. Banerjee, R. Gupta, and M. Mitra, “Delineation of ECG characteristic features using multiresolution wavelet analysis method,” *Measurement*, vol. 45, no. 3, pp. 474–487, Apr. 2012, doi: 10.1016/J.MEASUREMENT.2011.10.025.

[4] R. Hostettler, T. Lumikari, L. Palva, T. Nieminen, and S. Särkkä, “Motion Artifact Reduction in Ambulatory Electrocardiography Using Inertial Measurement Units and Kalman Filtering,” *2018*

21st International Conference on Information Fusion, FUSION 2018, pp. 780–787, Sep. 2018, doi: 10.23919/ICIF.2018.8455698.

[5] A. Aboalseoud *et al.*, "Wireless ECG Monitoring System for Telemedicine Application," 2019. Accessed: Mar. 23, 2022. [Online]. Available: https://ieeexplore-ieee-org.tudelft.idm.oclc.org/document/9014845/

[6] I. Romero, D. Geng, and T. Berset, "Adaptive filtering in ECG denoising: A comparative study," 2012. Accessed: Mar. 21, 2022. [Online]. Available: https://ieeexplore-ieee-org.tudelft.idm.oclc.org/document/6420326/

[7] F. A. Ghaleb, M. B. Kamat, M. Salleh, M. F. Rohani, and S. A. Razak, "Two-stage motion artefact reduction algorithm for electrocardiogram using weighted adaptive noise cancelling and recursive Hampel filter," *PLoS One*, vol. 13, no. 11, p. e0207176, Nov. 2018, doi: 10.1371/JOURNAL.PONE.0207176.

[8] J. G. Webster, "Reducing Motion Artifacts and Interference in Biopotential Recording," *IEEE Trans Biomed Eng*, vol. BME-31, no. 12, pp. 823–826, 1984, doi: 10.1109/TBME.1984.325244.

[9] N. Martini, M. Milanesi, N. Vanello, V. Positano, M. F. Santarelli, and L. Landini, "A real-time adaptive filtering approach to motion artefacts removal from ECG signals," *Int J Biomed Eng Technol*, vol. 3, no. 3–4, pp. 233–245, 2010, doi: 10.1504/IJBET.2010.032694.

[10] S. I. Patel, M. J. Souter, D. S. Warner, and M. A. Warner, "Equipment-related Electrocardiographic ArtifactsCauses, Characteristics, Consequences, and Correction," *Anesthesiology*, vol. 108, no. 1, pp. 138–148, Jan. 2008, doi: 10.1097/01.ANES.0000296537.62905.25.

[11] L.-M. Bai, M.-H. Fan, C.-H. Feng, and L.-H. Wang, "Using an Adaptive Filter to Remove ECG Motion Artifact Interference," 2018. Accessed: Mar. 23, 2022. [Online]. Available: https://ieeexplore-ieee-org.tudelft.idm.oclc.org/document/8448801/

[12] A. Gautam, Y.-D. Lee, and W.-Y. Chung, "Noise cancellation of electrocardiogram signal measured by wearable USN node," 2008. Accessed: Mar. 21, 2022. [Online]. Available: https://ieeexplore-ieee-org.tudelft.idm.oclc.org/document/4648057/

[13] Z. Zhang, I. Silva, D. Wu, J. Zheng, H. Wu, and W. Wang, "Adaptive motion artefact reduction in respiration and ECG signals for wearable healthcare monitoring systems," *Med Biol Eng Comput*, vol. 52, no. 12, pp. 1019–1030, Nov. 2014, doi: 10.1007/s11517-014-1201-7.

[14] W. Dargie, "A stochastic fusion technique for removing motion artefacts from the measurements of a wireless ECG," in *IEEE International Conference on Multisensor Fusion and Integration for Intelligent Systems*, 2016, vol. 0, pp. 449–454. doi: 10.1109/MFI.2016.7849529.

[15] M. Milanesi *et al.*, "Multichannel techniques for motion artifacts removal from electrocardiographic signals," *Annual International Conference of the IEEE Engineering in Medicine and Biology - Proceedings*, pp. 3391–3394, 2006, doi: 10.1109/IEMBS.2006.260464.

[16] F. Xiong, D. Chen, and M. Huang, “A Wavelet Adaptive Cancellation Algorithm Based on Multi-Inertial Sensors for the Reduction of Motion Artifacts in Ambulatory ECGs,” *Sensors 2020, Vol. 20, Page 970*, vol. 20, no. 4, p. 970, Feb. 2020, doi: 10.3390/S20040970.

[17] B. Widrow *et al.*, “Adaptive Noise Cancelling: Principles and Applications,” *Proceedings of the IEEE*, vol. 63, no. 12, pp. 1692–1716, 1975, doi: 10.1109/PROC.1975.10036.

[18] P. S. R. Diniz, “Adaptive filtering: Algorithms and practical implementation,” *Adaptive Filtering: Algorithms and Practical Implementation*, vol. 9781461441069, pp. 1–652, Nov. 2013, doi: 10.1007/978-1-4614-4106-9.

[19] J. Lilienthal and W. Dargie, “Comparison of Reference Sensor Types and Position for Motion Artifact Removal in ECG,” 2021. Accessed: Mar. 21, 2022. [Online]. Available: https://ieeexplore-ieee-org.tudelft.idm.oclc.org/document/9616221/

[20] P. Schober and L. A. Schwarte, “Correlation coefficients: Appropriate use and interpretation,” *Anesth Analg*, vol. 126, no. 5, pp. 1763–1768, May 2018, doi: 10.1213/ANE.0000000000002864.

[21] C. Beach, M. Li, E. Balaban, and A. J. Casson, “Motion artefact removal in electroencephalography and electrocardiography by using multichannel inertial measurement units and adaptive filtering,” *Healthc Technol Lett*, vol. 8, no. 5, pp. 128–138, 2021, doi: 10.1049/htl2.12016.

[22] B.-H. Kim, Y.-H. Noh, and D.-U. Jeong, “A Wearable ECG Monitoring System Using Adaptive EMD Filter Based on Activity Status,” 2015. Accessed: Mar. 23, 2022. [Online]. Available: https://ieeexplore-ieee-org.tudelft.idm.oclc.org/document/7096139/

[23] M. Pflugradt, S. Mann, V. Feller, Y. Lu, and R. Orglmeister, “Online learning algorithms for principal component analysis applied on single-lead ECGs,” *Biomedizinische Technik*, vol. 58, no. 2, pp. 121–130, Apr. 2013, doi: 10.1515/bmt-2012-0026.

[24] V. K. Pandey, “Adaptive filtering for baseline wander removal in ECG,” *Proceedings of the IEEE/EMBS Region 8 International Conference on Information Technology Applications in Biomedicine, ITAB*, 2010, doi: 10.1109/ITAB.2010.5687642.

[25] S.-H. Liu, “Motion artifact reduction in electrocardiogram using adaptive filter,” *J Med Biol Eng*, vol. 31, no. 1, pp. 67–72, 2011, doi: 10.5405/jmbe.676.

[26] S.-L. Koay, S.-J. Jung, and W.-Y. Chung, “Patient-specific adaptive neuro-fuzzy interference system motion artefacts cancellation for electrocardiogram signal over WSN,” *Sens Lett*, vol. 9, no. 2, pp. 786–790, 2011, doi: 10.1166/sl.2011.1615.

[27] Y.-H. Noh and D.-U. Jeong, “Implementation of fuzzy-rule based activity classification and optimized adaptive filter-set for wearable ECG Recording,” *International Journal of Multimedia and Ubiquitous Engineering*, vol. 7, no. 4, pp. 59–72, 2012, [Online]. Available: https://www.scopus.com/inward/record.uri?eid=2-s2.0-84868691208&partnerID=40&md5=fd3c4b3f31d8310723feff3081d840b7

[28] M. Huang, D. Chen, and F. Xiong, “An effective adaptive filter to reduce motion artifacts from ECG signals using accelerometer,” in *ACM International Conference Proceeding Series*, 2019, pp. 83–88. doi: 10.1145/3326172.3326214.

[29] H.-K. Jung and D.-U. Jeong, “Development of wearable ECG measurement system using EMD for motion artifact removal,” 2012. Accessed: Mar. 21, 2022. [Online]. Available: https://ieeexplore-ieee-org.tudelft.idm.oclc.org/document/6530346/

[30] Y.-S. O. Yang, W.-C. Lee, T.-C. Ke, C.-P. Wei, and C.-C. Lee, “Adaptive reduction of motion artefact in wireless physiological monitoring microsystems,” 2008. Accessed: Mar. 21, 2022. [Online]. Available: https://ieeexplore-ieee-org.tudelft.idm.oclc.org/document/4757161/

[31] N. Tasneem and I. Mahbub, “Dry Electrode Based Low-power ECG Acquisition System with Adaptive Motion Artifacts Cancellation,” 2020. Accessed: Mar. 21, 2022. [Online]. Available: https://ieeexplore-ieee-org.tudelft.idm.oclc.org/document/9184681/

[32] J. Lilienthal and W. Dargie, “Automatic Motion Artifact Removal in ECG with Canonical Polyadic Decomposition,” 2021. Accessed: Mar. 21, 2022. [Online]. Available: https://ieeexplore-ieee-org.tudelft.idm.oclc.org/document/9616139/

[33] M. A. D. Raya and L. G. Sison, “Adaptive noise cancelling of motion artifact in stress ECG signals using accelerometer,” in *Proceedings of the Second Joint 24th Annual Conference and the Annual Fall Meeting of the Biomedical Engineering Society] [Engineering in Medicine and Biology*, 2002, vol. 2. Accessed: Mar. 21, 2022. [Online]. Available: https://ieeexplore-ieee-org.tudelft.idm.oclc.org/document/1106637/

[34] D. A. Tong, K. A. Bartels, and K. S. Honeyager, “Adaptive reduction of motion artifact in the electrocardiogram,” in *Proceedings of the Second Joint 24th Annual Conference and the Annual Fall Meeting of the Biomedical Engineering Society] [Engineering in Medicine and Biology*, 2002, vol. 2. Accessed: Mar. 21, 2022. [Online]. Available: https://ieeexplore-ieee-org.tudelft.idm.oclc.org/document/1106451/

[35] T. Seol, S. Lee, and J. Lee, “A Wearable Electrocardiogram Monitoring System Robust to Motion Artifacts,” 2018. Accessed: Mar. 21, 2022. [Online]. Available: https://ieeexplore-ieee-org.tudelft.idm.oclc.org/document/8649897/

[36] S. W. Yoon, S. D. Min, Y. H. Yun, S. Lee, and M. Lee, “Adaptive motion artifacts reduction using 3-axis accelerometer in E-textile ECG measurement system,” *J Med Syst*, vol. 32, no. 2, pp. 101–106, Apr. 2008, doi: 10.1007/s10916-007-9112-x.

[37] D. Buxi *et al.*, “Correlation between electrode-tissue impedance and motion artifact in biopotential recordings,” *IEEE Sens J*, vol. 12, no. 12, pp. 3373–3383, 2012, doi: 10.1109/JSEN.2012.2221163.

[38] R. Bailón, L. Sörnmo, and P. Laguna, “A robust method for ECG-based estimation of the respiratory frequency during stress testing,” *IEEE Trans Biomed Eng*, vol. 53, no. 7, pp. 1273–1285, Jul. 2006, doi: 10.1109/TBME.2006.871888.

[39] M. M. Mukaka, “A guide to appropriate use of Correlation coefficient in medical research,” *Malawi Medical Journal*, vol. 24, no. 3, pp. 69–71, Oct. 2012, doi: 10.4314/mmj.v24i3.

[40] C. Yang and N. Tavassolian, “Motion Artifact Cancellation of Seismocardiographic Recording From Moving Subjects,” *IEEE Sens J*, vol. 16, no. 14, 2016, Accessed: Mar. 21, 2022. [Online]. Available: https://ieeexplore-ieee-org.tudelft.idm.oclc.org/document/7479480/

[41] A. Němcová, R. Smíšek, L. Maršánová, L. Smital, and M. Vítek, “A comparative analysis of methods for evaluation of ECG signal quality after compression,” *Biomed Res Int*, vol. 2018, 2018, doi: 10.1155/2018/1868519.

[42] D. Makowski *et al.*, “NeuroKit2: A Python toolbox for neurophysiological signal processing,” *Behav Res Methods*, vol. 53, no. 4, pp. 1689–1696, Aug. 2021, doi: 10.3758/S13428-020-01516-Y/TABLES/3.

[43] O. Banos *et al.*, “mHealthDroid: A novel framework for agile development of mobile health applications,” *Lecture Notes in Computer Science (including subseries Lecture Notes in Artificial Intelligence and Lecture Notes in Bioinformatics)*, vol. 8868, pp. 91–98, 2014, doi: 10.1007/978-3-319-13105-4_14/COVER.

[44] “Praxa Sense - Remote health monitoring to detect clinical disorders.” https://praxasense.com/ (accessed Sep. 11, 2022).

[45] G. D. Fraser, A. D. C. Chan, J. R. Green, and D. MacIsaac, “Removal of electrocardiogram artifacts in surface electromyography using a moving average method,” *MeMeA 2012 - 2012 IEEE Symposium on Medical Measurements and Applications, Proceedings*, pp. 128–131, 2012, doi: 10.1109/MEMEA.2012.6226621.

[46] M. A. F Pimentel *et al.*, “Wavelet transforms and the ECG: a review,” *Physiol Meas*, vol. 26, no. 5, p. R155, Aug. 2005, doi: 10.1088/0967-3334/26/5/R01.

[47] C. Xie, L. McCullum, A. Johnson, T. Pollard, B. Gow, and M. Benjamin, “Waveform Database Software Package (WFDB) for Python v4.0.0,” *PhysioNet* , 2022.

8 Appendixes

8.1 ECG and IMU plots

Examples of signals recorded with the WD Afi from the recording R7 while performing different physical activities is good to note that the X and Y axis in the particular device used for this recording were shifted from the other recordings.

8.1.1 Activity: Jumping

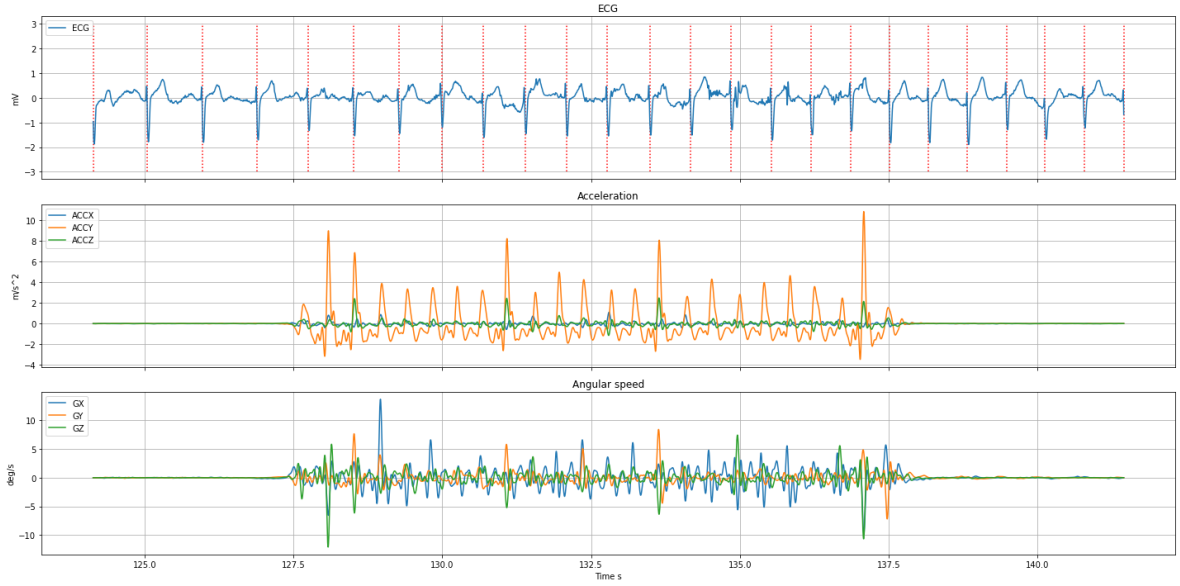

Figure 40. ECG, acceleration, and angular speed recorded with the wearable device while jumping.

8.1.2 Activity: Torso Rotations

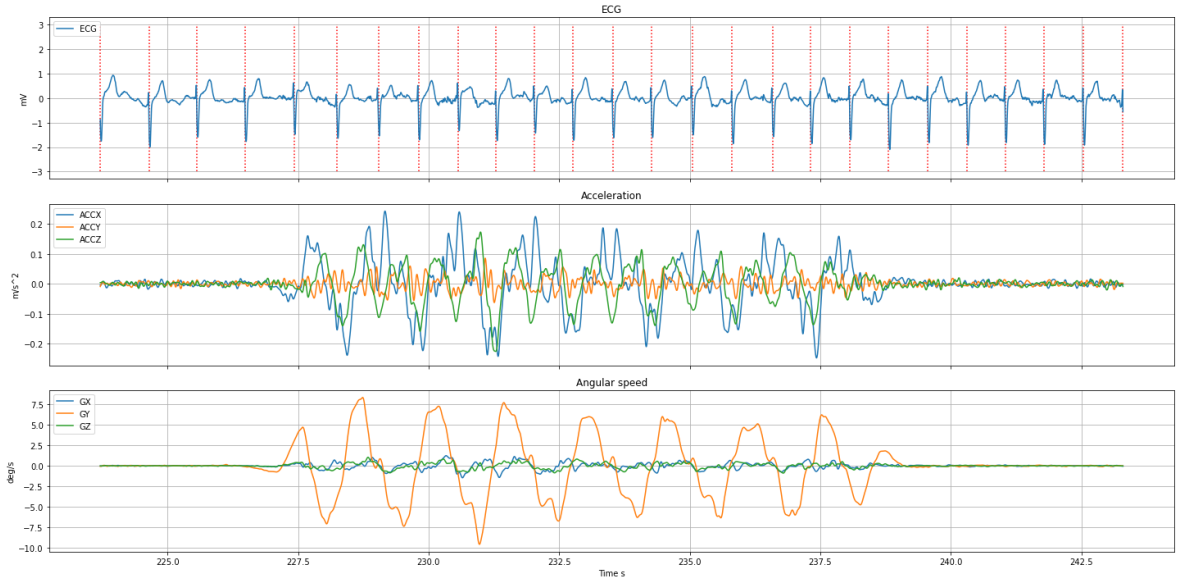

Figure 41. ECG, acceleration, and angular speed recorded with the wearable device while performing torso rotations.

8.1.3 Activity: Pushups

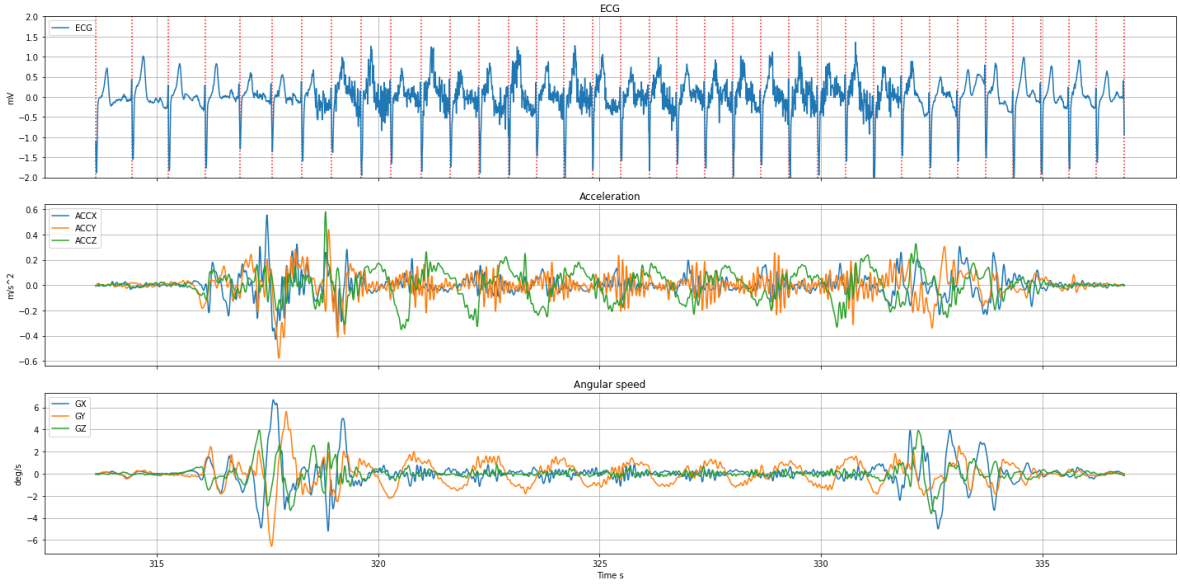

Figure 42. ECG, acceleration, and angular speed recorded with the wearable device while doing pushups.

8.1.4 Activity: Walking

Figure 43. ECG, acceleration, and angular speed recorded with the wearable device while walking.

8.1.5 Activity: Running

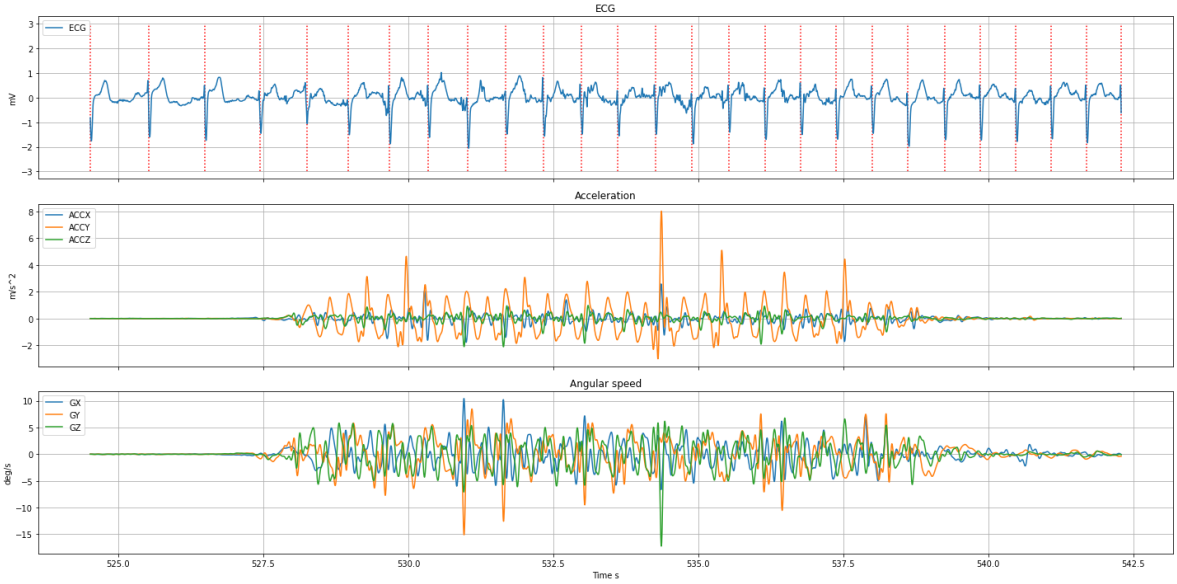

Figure 44. ECG, acceleration, and angular speed recorded with the wearable device while running.

8.2 Adaptive filter Python scripts

8.2.1 Least Means Squares

```
def LMS(x,r,N,K,mu):    #X signal of interest, r reference, N imput size, k filter order, mu constant

    w = np.zeros(K)                       # Initial filter taps
    e = np.zeros(N-K)
    for n in range(0, N-K):
        rn = r[n+K:n:-1]                  # Reference from n+K up to n backwards
        en = x[n+K] - np.dot(rn ,w)       # Error (Desired Signal) = primary imput - filter taps w . refetence imput rn
        w = w +   2 * mu * en * rn        # Update filter (LMS algorithm)
        e[n] = en                         # Error record
    e = np.append(np.zeros(K),e)
    return e
```

8.2.2 Normalized Least Means Squares

```
def NLMS(x,r,N,K,mu,g):    #X signal of interest, r reference, N imput size, k filter order, mu constant, g constant

    w = np.zeros((K,1))                       # Initial filter taps
    e = np.zeros(N-K)
    for n in range(0, N-K):
        rn = (np.array(r[n+K:n:-1])[np.newaxis]).T          # Reference from n+K up to n backwards
        en = x[n+K] - (rn.T@w)       # Error (Desired Signal) = primary imput - filter taps w . refetence imput rn
        w = w + ((mu*en) / (g + (rn.T@rn)))* rn         # Update filter (NLMS algorithm)
        e[n] = en                        # Error record
    e = np.append(np.zeros(K),e)
    return e
```

8.2.3 Recursive Least Squares

```
def RLS(x,r,N,k,d,L):#X signal of interest, r reference, N imput size, k filter order, d small constant, 0 >> L >= 1 constant

    sd= d*np.identity(k)
    e = np.zeros(N-k)
    w = np.zeros((k,1))                       # Initial filter taps
    for n in range(0, N-k):
        rn = (np.array(r[n+k:n:-1])[np.newaxis]).T          # Reference from n+K up to n backwards
        en = x[n+k] -(rn.T@w)
        f  = sd@rn
        sd = (1/L)*(sd-((f@f.T)/(L+((f.T)@rn))))
        w  = w + (en*sd@rn)
        e[n] = en                        # Error record
    e = np.append(np.zeros(k),e)
    return e
```

8.3 Filter performance

8.3.1 Afi Data

\

Jumping	SNR	Max Corr	ΔSNR LMS	ΔSNR NLMS	ΔSNR RLS	New Corr	ΔSNR LMS	ΔSNR NLMS	ΔSNR RLS	Δ Corr
R1	5.55	0.078	-2.69	-11.27	-0.91	0.087	-2.73	-17.8	-0.74	0.009
R2	7.99	0.87	-5.72	-1.88	-0.83	0.8	-6.05	-0.15	-0.78	-0.07
R3	7.06	0.077	-0.48	-0.02	-0.32	0.082	-0.45	-0.01	-0.26	0.005
R4	5.17	0.062	-2.09	-0.64	-0.21	0.061	-2.09	-0.03	-0.18	-0.001
R5	6.54	0.058	-2.27	-0.21	-0.29	0.064	-2.3	0.01	-0.24	0.006
R7	7.54	0.081	-174	-0.17	-0.16	0.084	-162	-0.01	-0.15	0.003
R8	5.87	0.554	0.86	-2.31	0.48	0.635	0.93	-2.26	0.67	0.081
Average	6.531	0.254	-26.627	-2.357	-0.320	0.259	-24.956	-2.893	-0.240	0.005

Torso Rotatios	SNR	Max Corr	ΔSNR LMS	ΔSNR NLMS	ΔSNR RLS	New Corr	ΔSNR LMS	ΔSNR NLMS	ΔSNR RLS	Δ Corr
R2	10.31	0.163	-0.12	-1.08	-0.62	0.16	-0.12	-0.01	-0.66	-0.003
R3	9.69	0.155	0.03	-0.14	-0.34	0.156	0.02	-0.3	-0.34	0.001
R4	9.24	0.179	-8.16	0.04	-0.96	0.179	-8.17	0.14	-0.94	0
R5	9.3	0.2	-7.81	-0.29	-0.92	0.2	-7.8	0.04	-0.89	0
R6	9.89	0.149	-8.58	-0.27	-1.85	0.149	-8.58	-0.28	-1.85	0
R7	9.94	0.337	0.149	-0.77	-0.41	0.346	0.16	0.014	-0.24	0.009
R8	10.6	0.155	-5.19	-0.34	-0.75	0.155	-5.22	-0.17	-0.81	0
Average	9.853	0.191	-4.240	-0.407	-0.836	0.192	-4.244	-0.081	-0.819	0.001

Pushups	SNR	Max Corr	ΔSNR LMS	ΔSNR NLMS	ΔSNR RLS	New Corr	ΔSNR LMS	ΔSNR NLMS	ΔSNR RLS	Δ Corr
R2	4.6	0.097	-2.96	-0.17	-0.24	0.096	-2.96	0.06	-0.24	-0.001
R3	7.68	0.099	-5.85	0.02	-0.04	0.099	-5.86	-0.1	-0.07	0
R4	5.03	0.105	-0.64	-1.92	-0.23	0.104	-0.67	-0.41	-0.19	-0.001
R5	7.45	0.104	-6.11	-0.27	-0.44	0.102	-6.11	-0.01	-0.46	-0.002
R6	-3.9	0.025	0	-0.11	-0.03	0.027	0	0	-0.03	0.002
R7	3.22	0.24	0.19	-1.42	0.12	0.24	0.18	-0.11	0.12	0
R8	3.74	0.119	-3.59	-0.02	-0.07	0.122	-3.56	-0.02	-0.09	0.003
Average	3.974	0.113	-2.709	-0.556	-0.133	0.113	-2.711	-0.084	-0.137	0.000

Walk	SNR	Max Corr	ΔSNR LMS	ΔSNR NLMS	ΔSNR RLS	New Corr	ΔSNR LMS	ΔSNR NLMS	ΔSNR RLS	Δ Corr
R1	11.45	0.113	-0.61	-5.4	-0.58	0.113	-0.61	-0.05	-0.58	0
R2	7.23	0.26	-0.23	-0.6	-0.32	0.268	0.23	0.16	-0.43	0.008
R3	4.73	0.131	-1.29	-0.02	-0.59	0.134	-1.22	0.01	-0.069	0.003
R4	7.79	0.162	-5.39	-2.06	-1.51	-0.162	-5.39	-0.35	-1.53	-0.324
R5	10.06	0.056	-7.17	-1.1	-1.97	0.059	-7.14	-0.04	-1.95	0.003
R7	8.51	0.089	-3.35	-2.25	-0.82	0.101	-3.37	-0.02	-0.9	0.012
R8	10.53	0.228	-6.81	0.05	-0.49	0.226	-6.8	0	-0.42	-0.002
Average	8.614	0.148	-3.550	-1.626	-0.897	0.106	-3.471	-0.041	-0.840	-0.043

Run	SNR	Max Corr	ΔSNR LMS	ΔSNR NLMS	ΔSNR RLS	New Corr	ΔSNR LMS	ΔSNR NLMS	ΔSNR RLS	Δ Corr
R2	4.68	0.12	-2.89	0.09	-0.85	0.131	-2.68	-0.02	-0.76	0.011
R3	4.84	0.098	-28.32	0.03	-0.91	0.065	-2.47	0.01	-0.31	-0.033
R4	8.77	0.174	-92.61	-0.75	-0.75	0.043	-4.49	-0.02	-0.69	-0.131
R5	8.61	0.168	-124	-0.12	-0.31	0.178	-69	0.06	-0.43	0.01
R6	6.76	0.088	-40.01	-0.07	-0.43	0.006	-3.21	-0.03	-0.2	-0.082
R7	8.41	0.142	-5.3	-1.04	-2.11	0.143	-5.28	0.01	-2.12	0.001
R8	8.77	0.323	-5.28	0.17	-0.41	0.323	-5.28	-0.18	-0.41	0
Average	7.263	0.159	-42.630	-0.241	-0.824	0.127	-13.201	-0.024	-0.703	-0.032

8.3.2 MHEALTH Data

Walk	SNR	Max Corr	ΔSNR LMS	ΔSNR NLMS	ΔSNR RLS	New Corr	ΔSNR LMS	ΔSNR NLMS	ΔSNR RLS	Δ Corr
MH2	**7**	**0.167**	-0.26	-0.03	-0.97	0.17	-0.27	-0.03	-0.85	0.003
MH3	**6.61**	**0.058**	-0.04	-0.02	-0.62	0.059	-0.03	-0.02	-0.64	0.001
MH4	**8.05**	0.023	-0.06	-0.02	-0.75	0.019	-0.02	-0.02	-0.24	-0.004
MH6	**8.94**	0.094	-0.01	-0.03	-0.64	-0.117	-0.02	-0.03	-0.61	-0.211
MH7	**6.76**	0.036	-0.07	-0.03	-0.72	0.012	-0.05	-0.03	-0.66	-0.024
Average	**7.472**	**0.076**	**-0.088**	**-0.026**	**-0.740**	**0.029**	**-0.078**	**-0.026**	**-0.600**	**-0.047**
Jump	**SNR**	**Max Corr**	**ΔSNR LMS**	**ΔSNR NLMS**	**ΔSNR RLS**	**New Corr**	**ΔSNR LMS**	**ΔSNR NLMS**	**ΔSNR RLS**	**Δ Corr**
MH2	**5.04**	0.114	-0.28	-0.07	2.31	0.11	-0.16	-0.07	-1.65	-0.004
MH3	**6.82**	0.127	-0.839	-0.03	-1.52	-0.093	-0.6	-0.03	-1.63	-0.22
MH4	**6.05**	0.134	-4.17	-0.149	-2.23	-0.131	-3.75	-0.149	-1.889	-0.265
MH6	**6.85**	0.211	-4.59	-0.08	-3.42	-0.173	-3.14	-0.09	-3.55	-0.384
MH7	**7.28**	0.042	-3.92	-0.11	-2.3	0.046	-1.76	-0.11	-2.27	0.004
Average	**6.408**	**0.1256**	**-2.7598**	**-0.0878**	**-1.432**	**-0.0482**	**-1.882**	**-0.0898**	**-2.1978**	**-0.1738**
Run	**SNR**	**Max Corr**	**ΔSNR LMS**	**ΔSNR NLMS**	**ΔSNR RLS**	**New Corr**	**ΔSNR LMS**	**ΔSNR NLMS**	**ΔSNR RLS**	**Δ Corr**
MH2	**-1.23**	0.125	-2.6	-0.13	-1.47	0.098	-2.3	-0.13	-1.38	-0.027
MH3	**4.37**	0.068	-0.669	-0.009	-1.13	0.041	-0.35	-0.009	-0.77	-0.027
MH4	**6.51**	0.062	-0.55	-0.02	-0.74	0.061	-0.16	-0.02	-0.679	-0.001
MH6	**5.6**	0.177	-2.54	0.02	-0.15	0.086	0.06	-0.01	-0.29	-0.091
MH7	**7.54**	0.104	-0.92	-0.01	-1.84	0.044	-0.48	-0.01	-1.68	-0.06
Average	**4.558**	**0.107**	**-1.456**	**-0.030**	**-1.066**	**0.066**	**-0.646**	**-0.036**	**-0.960**	**-0.041**
Squat	**SNR**	**Max Corr**	**ΔSNR LMS**	**ΔSNR NLMS**	**ΔSNR RLS**	**New Corr**	**ΔSNR LMS**	**ΔSNR NLMS**	**ΔSNR RLS**	**Δ Corr**
MH2	**5.26**	0.088	0.02	-0.03	-0.3	0.058	-0.01	-0.03	-0.3	-0.03
MH3	**4.67**	0.095	-0.04	-0.03	-0.379	0.068	-0.03	-0.03	-0.36	-0.027
MH4	**6.86**	0.063	-0.14	-0.02	-0.879	0.039	-0.11	-0.02	-0.77	-0.024
MH6	**8.5**	0.104	0.3	0	-0.97	-0.07	0.11	-0.03	-1.07	-0.174
MH7	**6.51**	0.085	-0.02	-0.02	-0.86	0.098	-0.02	-0.02	-0.93	0.013
Average	**6.360**	**0.087**	**0.024**	**-0.020**	**-0.678**	**0.039**	**-0.012**	**-0.026**	**-0.686**	**-0.048**